Droplet breakup mechanisms in premix membrane emulsification and related microfluidic channels

Droplet breakup mechanisms in premix membrane emulsification and related microfluidic channels

Akmal Nazir[1,*], Goran T. Vladisavljević[2]

[1]Department of Food Science, College of Food and Agriculture, United Arab Emirates University, Al Ain (15551), UAE

[2]Chemical Engineering Department, Loughborough University, Loughborough, Leicestershire LE11 3TU, UK

*Email: akmal.nazir@uaeu.ac.ae

ABSTRACT

Premix membrane emulsification (PME) is a pressure driven process of droplet breakup, caused by their motion through membrane pores. The process is widely used for high-throughput production of sized-controlled emulsion droplets and microparticles using low energy inputs. The resultant droplet size depends on numerous process, membrane, and formulation factors such as flow velocity in pores, number of extrusions, initial droplet size, internal membrane geometry, wettability of pore walls, and physical properties of emulsion. This paper provides a comprehensive review of different mechanisms of droplet deformation and breakup in membranes with versatile pore morphologies including sintered glass and ceramic filters, SPG and polymeric membranes with sponge-like structures, micro-engineered metallic membranes with ordered straight-through pore arrays, and dynamic membranes composed of unconsolidated particles. Fundamental aspects of droplet motion and breakup in idealized pore networks have also been covered including droplet disruption in T-junctions, channel constrictions, and obstructed channels. The breakup mechanisms due to shear interactions with pore walls and localized shear (direct breaking) or due to interfacial tension effects and Rayleigh-Plateau instability (indirect breaking) were systematically discussed based on recent experimental and numerical studies. Non-dimensional droplet size correlations based on capillary, Weber, and Ohnesorge numbers were also presented.

Keywords: Membrane emulsification, microfluidic channel, droplet breakup, non-dimensional correlations

Contents

1. Introduction

Emulsions are dispersions of two or more immiscible liquids in which one is dispersed as small droplets in the other [1]. Over the last two decades, a tremendous advancement is witnessed in emulsion science, which has been well acknowledged in food, pharmaceutical, cosmetic, and chemical industry for the preparation of pharmaceutical, food and cosmetic products [2], encapsulation and delivery of bioactive components [3], and for synthesis of micro-/nanomaterials [4]. The energy-intensive conventional systems, such as high-pressure homogenizers and high shear rotor-stator systems, are characterized by high throughputs but with a limited control over mean droplet size and uniformity [5]. As majority of applied energy is dissipated as heat, and droplet breakup greatly relies on high shear fields; therefore, these techniques are less suitable for heat and shear sensitive ingredients, and for applications where a strict control over droplet size is required. These constraints have led to an unprecedented development of various microstructured emulsification devices, which can be broadly classified into membrane and microfluidic systems [6]. The microstructured devices provide a better control over droplet generation process and require energy inputs that are orders of magnitude lower compared to conventional techniques. Microfluidic emulsification systems are basic elements of advanced lab-on-a-chip technologies that offer multitudinous applications in life sciences [7]. However, their utilization is still limited to highly sophisticated applications due to low throughputs (typically less than 1 ml/h of the dispersed phase for droplet sizes of less than 20 μm) and costly microfabrication processes. Remarkably, membrane emulsification can bridge the gap between the two extremities by promising high throughput (as of conventional systems) and precise droplet breakup (as of microfluidic systems). In a typical direct membrane emulsification (DME) process, to-be-dispersed phase is pushed through membrane pores at controlled injection rate and shear conditions that results in reproducible droplet formation on downstream side of the membrane, which is in contact with cross-flowing [8] or stirred continuous phase [9]. In premix membrane emulsification (PME) a coarse emulsion (premix) is extruded through a membrane to get a fine emulsion by droplet breakup within a porous structure (Fig. 1). The droplet size in DME is at least double of a pore size, whereas in PME a droplet size less than half of pore size can be achieved easily under optimum conditions [10]. This is due to much larger shear, extensional, and impact forces leading to an effective droplet disruption [11]. A crucial difference between DME, PME and conventional emulsification devices is that DME is based on drop-by-drop manufacturing, PME relies on droplet break-up in membrane pores (whose size is of the same order of magnitude as size of resultant

droplets), while conventional emulsification is achieved in the reaction space which is at least several orders of magnitude larger than the size of resultant droplets.

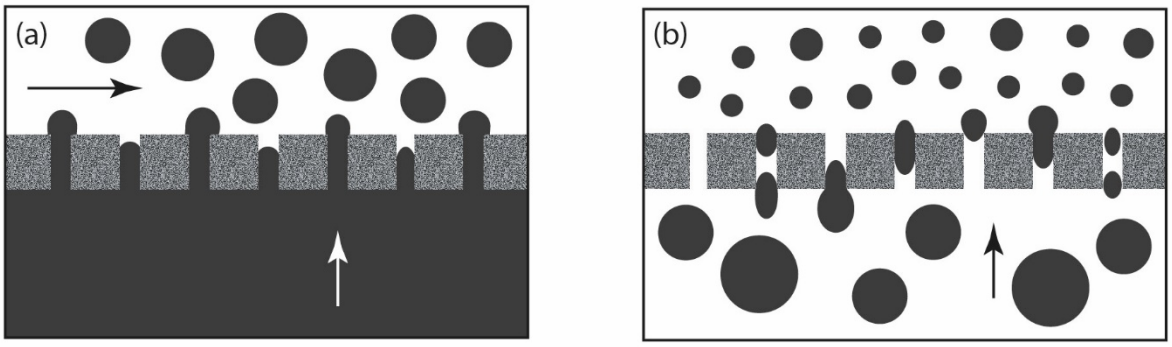

Fig. 1. Schematic representation of (a) direct membrane emulsification (DME) and (b) premix membrane emulsification (PME). The direction of fluid flow is represented by arrows. The to-be-dispersed and continuous phases are represented by black and white colours, respectively. The membrane position is shown by gray shading.

The success of PME over DME lies in simplicity of its operation because there is no need for cross-flow pump or emulsion recirculation (but repeated passes through a membrane may be needed), short emulsification time, high throughputs, ability to handle both small and large liquid volumes and to obtain much smaller droplet to pore size ratios than in DME, and possibility to achieve simultaneous phase inversion and droplet disruption. As a result, PME received an increasing attention of researchers working in the domain of encapsulation and material science, who have fabricated various novel dispersions and particulate products all the way down to nanoscale through this technique (Table A.1). Compared to traditional devices for high-energy preparation of nanoemulsions such as microfluidizers and ultrasonic homogenizers, PME typically generates nanodroplets without any micron-sized droplet fractions, which can promise a higher storage stability even at elevated temperatures and under stressed conditions [12] However, the concentration of free surfactant in the continuous phase, which should be very low to minimize micellar-transport-driven Ostwald ripening [13]. PME can easily achieve extremely small droplet sizes of just 100 nm using membranes with very small pore sizes (100 nm or less), transmembrane pressure typically around 10 bar, and suitable surfactants [14].

The membrane is a crucial component of a PME system in which droplet disruption takes place. The required hydrodynamic conditions inside membrane are generated through feed emulsion flow that is driven by transmembrane pressure. Usually, a smaller pore size and higher flow velocities inside pores (especially at lower interfacial tension and lower dispersed to continuous-phase viscosity ratio) lead to more extensive droplet break-

up and smaller droplet size after disruption. However, microstructural and surface properties of membrane, such as its thickness, porosity, electrical charge, wettability, and pore shape, tortuosity, and interconnectivity, are also important to control the process. The final droplet size is an interplay of various disruptive forces (due to shear and system geometry) and restoring forces (due to interfacial tension) that are quite difficult to quantify. The effect of different process and formulation parameters on droplet formation in PME can be found in previous reviews [10, 11]. However, over the last decade, various membranes, porous media (consisted of unconsolidated particles or stacked flow obstacles), and microfluidic channel networks have been used for droplet breakup, each with some distinct features. Moreover, novelties in system design and operation of PME are reported to make the process more flexible and practically feasible. The present article aims at critically analyzing the latest developments related to the fundamental principles of the process and droplet breakup mechanisms in PME. Various dimensionless numbers and scaling relations are summarized, which are quite useful to characterize flow behavior and droplet breakup in PME. Furthermore, droplet breakup in microfluidic channels (with well-defined system geometry and visual observation of droplets) is presented to gain more insight into fundamental aspects of PME. Some practical information related to fouling and cleaning of membranes is also provided towards the end of the article.

2. Process design and operation

PME was introduced towards end of the 20th century by Suzuki et al [15] to produce fine O/W emulsions from pre-emulsified O/W mixtures using a microporous glass membrane (MPG) with a pore size of 2.7 or 4.2 μm. After that, they used hydrophilic and hydrophobic polytetrafluoroethylene (PTFE) membranes with a pore size of 1 μm to homogenize O/W and W/O emulsions, respectively [16]. Furthermore, PTFE membranes were used to produce concentrated O/W and W/O emulsions through phase inversion, i.e., a process that converts a coarse O/W emulsion into a fine W/O emulsion when passed through a hydrophobic membrane, and *vice versa* [17]. These proof-of-principle studies paved a way for numerous subsequent investigations using many different membrane materials and emulsion formulations.

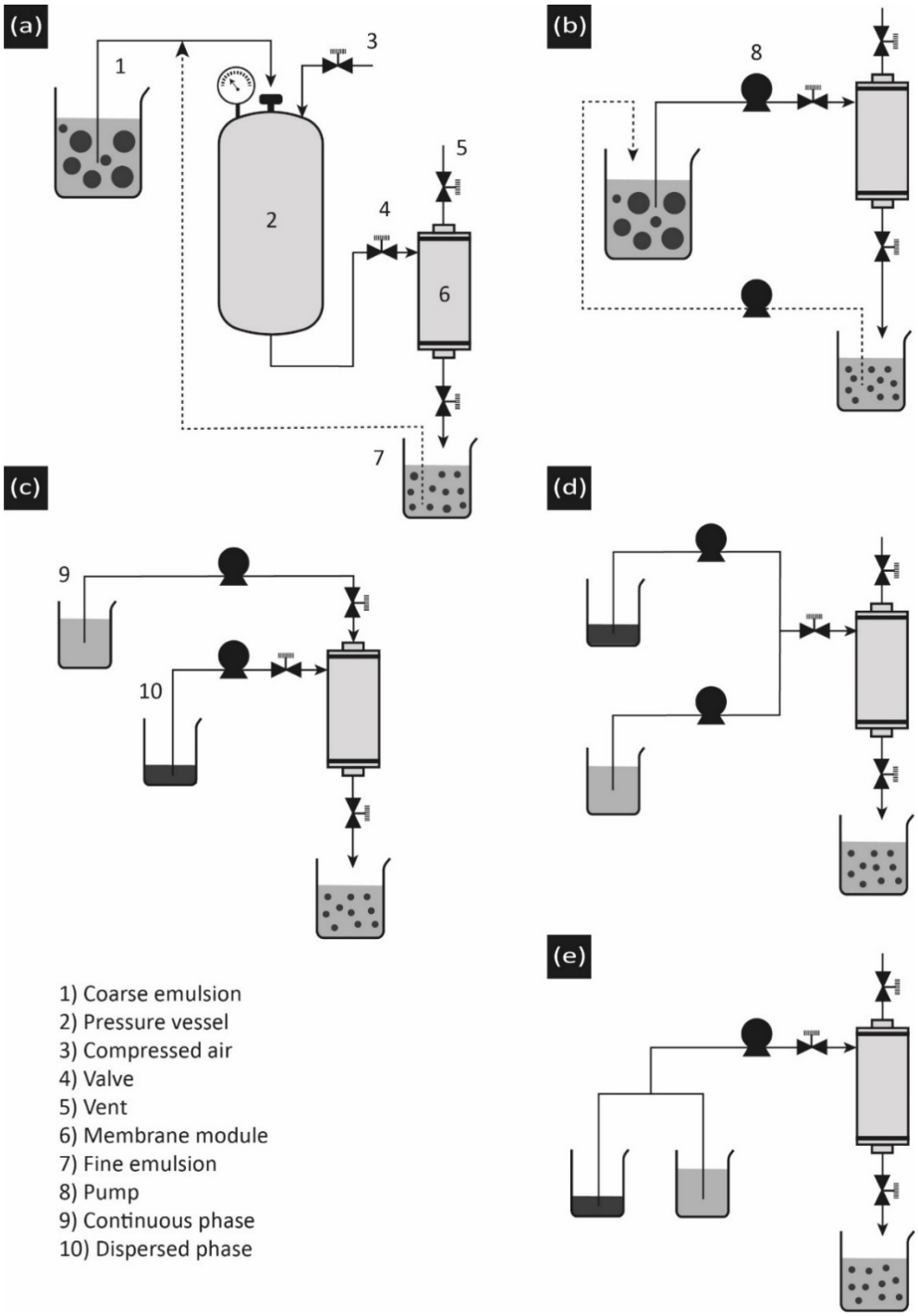

Fig. 2. A schematic representation of different designs of PME systems: (a) The coarse emulsion is injected into membrane module through a pressurized vessel [18, 19]; (b) The coarse emulsion is injected into membrane module through a pump [20], (c) The to-be-dispersed and continuous phases are injected separately into the module by using two pumps [21], (d and e) The to-be-dispersed and continuous phases are drawn simultaneously by one or two pumps and the coarse emulsion is formed inside the flow channel before entering into the membrane module [22]. The dotted lines in (a) and (b) represent an optional step for recycling of the emulsion for certain number of times.

A typical PME system consists of a pressure vessel (that contains coarse emulsion) and a dead-end module to hold a membrane [18]. At the beginning of the process, all air pockets on high-pressure side of the membrane should be removed to expose the membrane surface fully to the feed emulsion. The coarse emulsion is then pressurized (e.g., in a pressure vessel or through a pump) and extruded through membrane to break larger droplets into smaller ones (Fig. 2a,b). The modules with flat [23] and tubular [15] membranes can be used, as well as a packed bed of glass beads [19]. In order to get uniform emulsion droplets, the emulsification cycle is usually repeated for a number of times, as shown by dotted lines in Fig. 2a,b. In preparation of double emulsions, repeated extrusions may result in coalescence of internal droplets, which can be used to fine-tune morphology of double emulsion droplets prepared by PME from multi-core to single-core [24]. Multiple extrusions are usually carried out manually (if a pressure vessel is used) or the extruded emulsion is recycled back into the module by a recirculating pump (if another pump is used to pressurize coarse emulsion). For this reason, PME could work in batch as well as in continuous mode.

A PME system can be provided with gentle stirring on downstream side of the membrane to generate external shear and to keep newly formed droplets in a continuous motion. This can ensure emulsion stability as it prevents creaming and reduces droplet coalescence, until newly formed droplet interfaces are stabilized with surfactant molecules [25]. The agitation of the product emulsion can also be achieved by cross flow on downstream side of the membrane or by using dynamic membranes (oscillating or rotating) [26], but this approach was rarely used in PME.

PME is a two-step emulsification process involving primary homogenization (preparation of coarse emulsion) and secondary homogenization (preparation of fine emulsion). The coarse emulsion can be prepared by simply mixing dispersed and continuous phases with magnetic bar or impeller. The optimum stirring speed was found between 400-600 rpm [27]. High stirring speed (800 rpm or above) should be avoided as it may lead to large fraction of small droplets that can freely pass through membrane pores leading to a broad particle size distribution after PME [28]. The coarse emulsion can be also prepared by DME using a membrane with a significantly larger pore size than the membrane used subsequently in PME [29, 30]. For continuous operation or to avoid loss of sensitive ingredients (that may occur in mechanical homogenization devices during premix preparation), an inline PME was proposed by Nazir [21] as shown in Fig. 2c. In this system, dispersed and continuous phases are simultaneously injected into the membrane module through separate nozzles. The two streams meet each other and form a coarse emulsion inside the module, which is then passed through membrane under the prevailing pressure conditions. Hence, an additional energy is not needed for preparation of coarse emulsion apart from kinetic energy of two impinging

liquid streams. The concentration of dispersed phase can be regulated by controlling flow rates of both phases. A slightly modified approach (termed as intramembrane PME) was later proposed by Mugabi et al [22], wherein the premix is formed inside the flow channel before entering the membrane module (Fig. 2d,e).

Furthermore, PME can be achieved using a two-syringe membrane emulsification (2SME) technique [31] based on extrusion of feed emulsion through the membrane placed between two syringes. The process can be facilitated using syringe extruders, such as Avanti® Mini-Extruder [32], which is commonly used for preparation of lipid vesicles and solid lipid nanoparticles [34]. To obtain a deeper insight into PME process, instrumented small-scale extruders can be used with computer-controlled syringe pumps and integrated pressure sensors to record extrusion pressure continuously during the process [33].

3. Membranes and porous media used in PME

As already stated, a membrane is the most critical component in PME that is largely responsible for droplet deformation and breakup. Therefore, an appropriate selection of membrane is indispensable to carry out desired emulsification process. Until now, various organic and inorganic membranes and porous media such as packed beds of unconsolidated particles, have been used for PME, which are categorized and discussed below.

3.1. Glass and ceramic membranes

Glass membrane can be fabricated by sintering quartz and borosilicate glass powder or through phase separation in borosilicate glasses. Both types of porous glasses have been used in PME. Shirasu Porous Glass (SPG) membrane (SPG Technology Co., Ltd., Japan) is mainly composed of Al_2O_3–SiO_2 skeleton with tortuous interconnected pores, as shown in Fig. 3. The SPG membrane is usually fabricated from a Na_2O–CaO–MgO–Al_2O_3–B_2O_3–SiO_2 mother glass through phase separation caused by spinodal decomposition process at elevated temperature, and a subsequent acid (HCl) leaching of $CaCO_3$–B_2O_3 [34]. Additionally, ZrO_2 can be added to the mother glass to improve the resistance of glass to alkali [34]. The SPG membrane has high mechanical, chemical and thermal strength, and is available in various shapes (flat disc or tubular) and with different pore sizes (0.04–40 μm), porosities (50-60%), and wettability types (hydrophilic or hydrophobic) [35]. The hydrophobic SPG membrane is made through surface modification of the original (hydrophilic) SPG membrane through suitable chemical or physical procedures [36]. The SPG membranes have been extensively used in PME due to ease of surface treatment and high pore interconnectivity that helps in droplet break-up. It is beyond the scope of this paper to review all

studies in which SPG membranes were used; however, some selected studies are summarized in Table A.1 to show the extent of applicability of SPG membrane in PME. The data presented in Table A.1 show the compatibility of SPG membranes to a range of ingredients and production protocols, to produce micro/nano-scaled materials.

Apart from SPG, other types of microporous glass (MPG) membranes are also reported in literature. For instance, MPG membrane developed by ISE Chemical Industries Co., Ltd. (Japan) was used in the first PME study [15], and in some DME studies [37-40]. Another MPG membrane, developed by Senhui Microsphere Tech. Co., Ltd. (China), has been reported for the formation of various micro-/nanoparticles through PME [41-45].

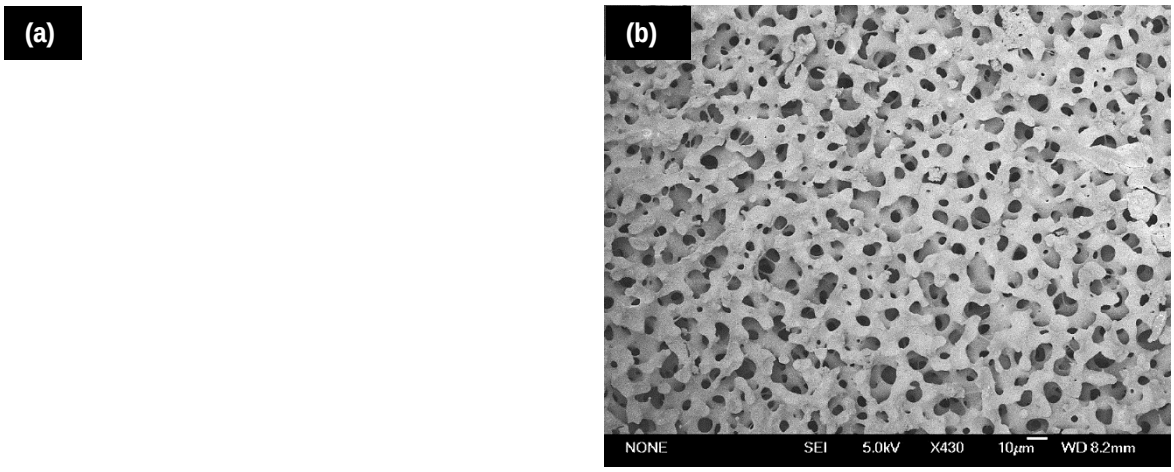

Fig. 3. SEM images of (a) top surface, and (b) cross section of SPG membrane with a pore size of 10.2 μm [46].

Closely related to glass membranes are the ceramic membranes that are fabricated from inorganic materials such as aluminum oxide (Al_2O_3), zirconium oxide (ZrO_2), titanium oxide (TiO_2), mullite ($3Al_2O_3{\cdot}2SiO_2$), and silicon oxycarbide (SiOC). The use of ceramic membranes is advantageous because of their high porosity, high chemical resistance, and stability against extreme temperatures and pH conditions. The first PME study with ceramic membranes was reported by Jing et al [25], who produced toluene droplets dispersed in 2 wt% sodium dodecyl sulfate (SDS) solution through two types of laboratory made ceramic membranes: ZrO_2 (pore size: 0.16 μm) and Al_2O_3 (pore size: 1.5 and 5 μm). Due to smaller pore size, the emulsification was not possible through ZrO_2 membrane (even at 250 kPa), whereas successful jet formation took place out of both Al_2O_3 membranes (the critical jet emulsion pressure was 140 and 70 kPa, respectively).

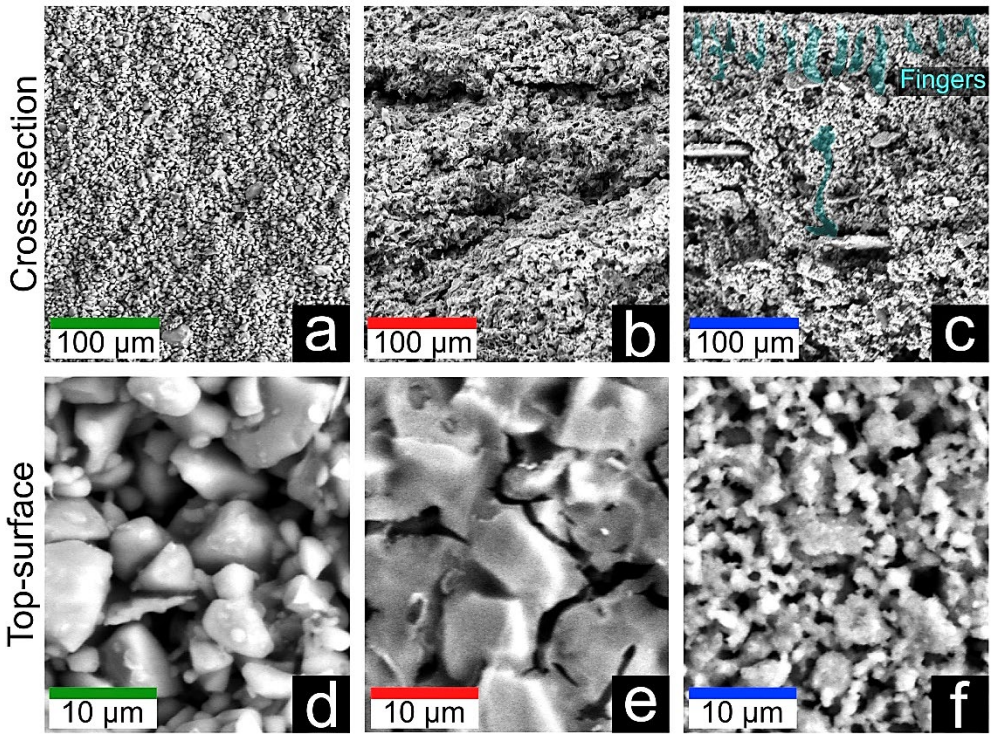

Fig. 4. SEM images of cross-sectional and top surface of (a,d) symmetric membrane with sintered non-spherical borosilicate glass fragments (VitraPOR® Sinterfilter, ROBU® Glasfilter-Geräte, Por. 5, pore size: 1.0-1.6 µm); (b,e) symmetric silicon oxycarbide (SiOC) membrane (pore size: 1.8 µm); and (c,f) asymmetric mullite membrane (pore size: 1.2 µm) manufactured from polymethylsiloxane and aluminum diacetate [47, 48].

Nishihora et al [47] prepared O/W emulsions of medium-chain fatty acid triglycerides using a commercially available glass membrane (borosilicate, symmetric, pore size: 1.39 µm) and two lab-made ceramic membranes: SiOC (symmetric, pore size: 1.76 µm) and mullite (asymmetric, pore size: 1.2 µm), as shown in Fig. 4. Another borosilicate membrane (commercial, symmetric, pore size: 40–100 µm) was used as a support membrane in the emulsification setup. All glass and ceramic membranes were able to produce emulsions with droplet size of less than 5 µm with a monomodal size distribution (droplet span < 1). An important finding of this study was the comparison between symmetric and asymmetric structures for PME. The thickness of the top layer of asymmetric mullite membrane was around 6.1 µm, whereas the other two symmetric membranes were 1000 µm thick. Despite this, mullite membrane showed comparable results for droplet size and uniformity, and with a superior flux performance compared to the symmetric membranes. This highlights the importance of constriction effect that dominates the droplet breakup mechanism during PME, which is discussed in more detail in Section 4 and 5.

3.2. Polymeric membranes

Various polymeric microfiltration membranes made of polytetrafluoroethylene (PTFE), polycarbonate (PC), polyethylene (PE), polysulfone (PS), polyethersulfone (PES), cellulose mixed esters (MCE), cellulose acetate (CA), polyvinylidene fluoride (PVDF), epoxy-based polymer (EP), and nylon, were used for PME [17, 49-54], as shown in Fig. 5. The polymeric membranes are usually fabricated by different methods such as sintering, track-etching, phase inversion, phase separation, electrospinning, etc. [55, 56]. Based on the fabrication material and procedure, the resulting membranes may have different structures (symmetric or asymmetric), pore geometry (cylindrical straight-through, spongy, branched cylindrical or rectangular pores [57]), pore size, wettability, strength, etc. Therefore, the commercial polymeric membranes are available with a wide range of specifications and are usually inexpensive (often used as a disposable material). A support sieve or mesh is usually required for polymeric membrane to withstand the transmembrane pressure during emulsification.

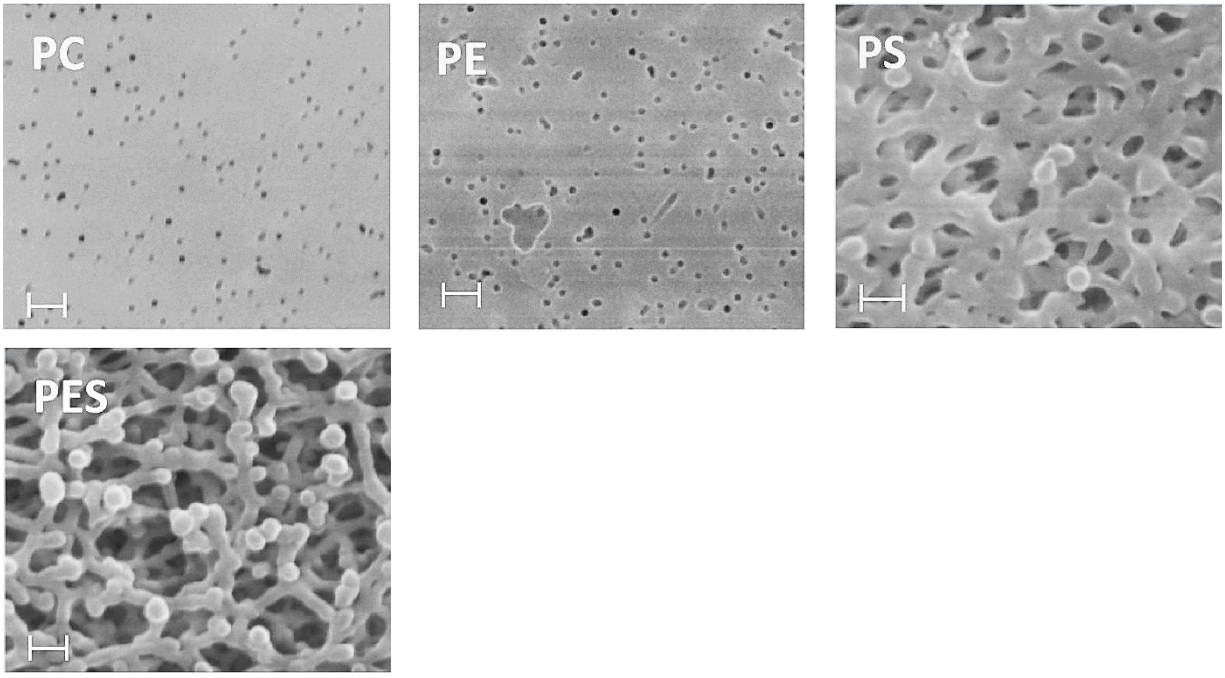

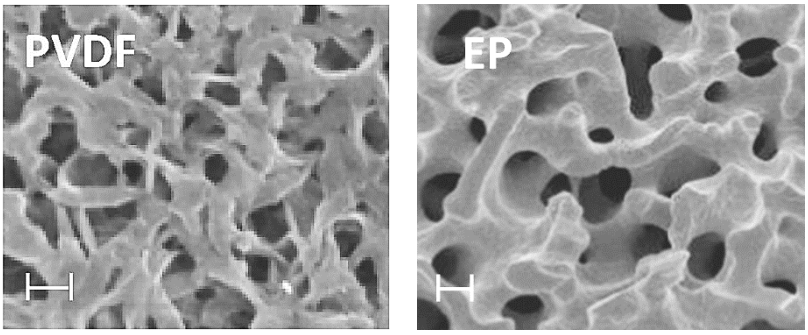

Fig. 5. SEM images of some polymeric membranes used in PME [36, 52]: track-etched polycarbonate (PC) and polyester (PE) membranes with cylindrical pores (thickness: 10 μm, pore size: 200 nm); polysulfone (PS), polyethersulfone (PES), cellulose acetate (CA), and nylon membranes with branched and interconnected pores (thickness: ~150 μm, pore size: 200 nm); epoxy-based polymer (EP) membrane with 3D bicontinuous skeleton structure and elliptical pores (thickness: 2 mm, pore size: 1.22 μm); polytetrafluoroethylene (PTFE) membrane with spongy structure (pore size: 0.22 μm). For all the images, the scale bar is equal to 1 μm.

Trentin et al [54] were the first who studied different polymeric microfiltration membranes (PC, PES, MCE and nylon) for PME for the preparation of O/W emulsions stabilized by Tween 20 (a low-molecular weight non-ionic surfactant) or bovine serum albumin (BSA) protein. The successful emulsification was observed under certain combinations of transmembrane pressure and pH, varied form 1-9 bar and 5.8-8.0, respectively. It is always trickier to use proteins in PME in general, due to an increased risk of membrane fouling and due to a smaller reduction in interfacial tension of droplets. It will reduce the flow rate of droplets through the membrane (because of higher Laplace pressure), and as a result, the droplet concentration inside the membrane increases. In addition, the electrostatic interactions between proteins and polymeric membrane may further worsen the condition. Therefore, a combination of a low molecular surfactant (i.e., Tween 20) and protein is beneficial to achieve higher transmembrane fluxes and higher droplet stabilization, as interfacial adsorption rate for low molecular weight surfactants is much faster than that of protein molecules [58]. Gehrmann and Bunjes [52] reported the preparation of O/W nanoemulsions using different polymeric membranes (pore size: 200 nm) and surfactants. A combination of different materials resulted in emulsions having different median droplet size (0.08-11 μm), while the droplet size span was around 0.6 for most of the cases. Notably, a submicron droplet size could only be achieved by using an appropriate combination of emulsifier and membrane material; however, the membrane structure or thickness were found less relevant after 21 extrusion cycles. The nylon and CA membranes gave submicron emulsions with all emulsifiers, whereas, rest of the membranes gave submicron emulsions only with certain emulsifiers (Fig. 6a).

The interaction of surfactant and membrane material can be explained in terms of the angle that is formed by the edge of a continuous phase droplet placed on a horizontal membrane [52] (Fig. 6b). If the contact angle between a polymeric membrane and continuous phase was less than 49° (i.e., the membrane was strongly wetted with the emulsifier solution), the median droplet size of O/W emulsion after 21 extrusions was always less than 500 nm; whereas, for more than 55° contact angle the droplet size was above 1 μm in all the cases. The role of wettability in producing submicron droplets was reconfirmed by comparing a commercial anodic alumina membrane (Al_2O_3, pore size: 200 nm, Whatman® Anodisc™) and hydrophilized or native PE and PC membranes with the same pore morphology. The hydrophilized PE and PC membranes performed better that the untreated polymeric membranes indicating that the contact angle was more relevant than the pore structure. Al_2O_3 membrane was able to generate a small median droplet size (<250 nm) with all emulsifiers with relatively high transmembrane fluxes. The improved performance of Al_2O_3 membrane was attributed to a highly hydrophilic surface (the contact angle between pure water and membrane surface was too low to be measured).

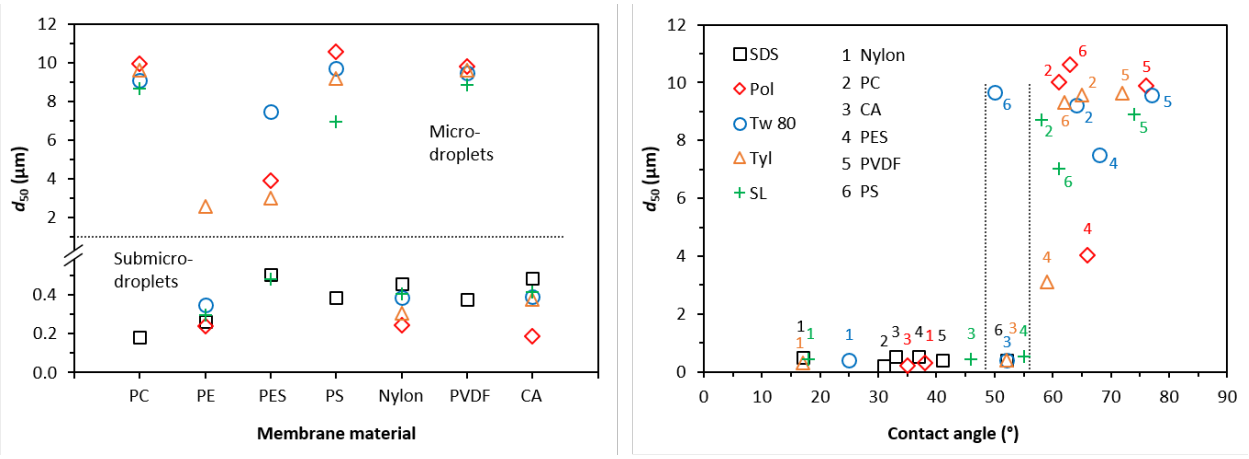

Fig. 6. The median droplet size, d_{50}, of medium chain fatty acid triglyceride-based emulsions produced using different polymeric membranes with a pore size of 200 nm and different surfactants after 21 extrusions through each membrane at the flow rate of 0.25 ml/s [52].

The polymeric membranes were also used for the preparation of solid micro-/nanoparticles via O/W emulsification. Ramakrishnan et al [53] prepared fish oil microcapsules through PME and subsequent spray drying using MCE and nylon membranes (pores size: 0.8 μm) using different concentrations of whey protein isolates and maltodextrin in the continuous phase. Joseph and Bunjes [49] prepared solid lipid nanoparticles of trimyristin using PC membranes through melt PME. The emulsions were generated at temperatures above the melting point of trimyristin and the droplets were subsequently solidified by cooling the product emulsions to 5°C.

The availability of polymeric membranes that are inherently hydrophobic is advantageous for the preparation of W/O emulsions, as no prior surface modification is needed. Zhou et al [46] produced agarose beads through W/O emulsification using hydrophobic PE membrane. The pore size distribution and shape of the pores did not affect the droplet size uniformity over a wide range of experimental conditions. However, the contact angle between membrane surface and water phase had a significant impact on the droplet size distribution, which is analogous to the observation in O/W emulsification process. A more hydrophobic membrane with a contact angle above 120°, while keeping other parameters constant, would always deliver a narrow droplet size distribution of W/O emulsions. The same research group reported preparation of W/O emulsions through another hydrophobic membrane, i.e., epoxy-based polymer (EP) membrane prepared by polymerization-induced phase separation [36, 59]. The produced W/O emulsion droplets were subsequently transformed into Ca-alginate microspheres having coefficient of variance of 11.4% by mixing with a $CaCl_2$ mini-emulsion. The hydrophobic EP membranes with 3D bicontinuous skeleton structures and narrow pore size distribution were found more effective in producing uniform W/O emulsions and more stable against alkalis, as compared to PE and SPG membranes [60].

3.3. Metallic membranes

The metallic membranes are preferred because of their high thermal and mechanical stability. Nickel and stainless steel are commonly used materials for fabricating metallic membranes (Fig. 7). The micro-engineered metallic membranes have well-defined straight-through pores with regular surface arrangement and a narrow pore size distribution. Due to a sieve-like design, metallic membranes are less prone to depth fouling as compared to sintered and phase separated glass, ceramic and polymeric membranes. A drawback of laser-drilled metallic membranes is their low porosity that limits the emulsification rate. However, a less porous structure is more suitable for DME where chances of coalescence between emerging droplets are minimized, which leads to formation of highly monodispersed emulsions. The metallic membranes are usually hydrophilic in nature, but can be made hydrophobic through surface modification or coating with a suitable polymer [61].

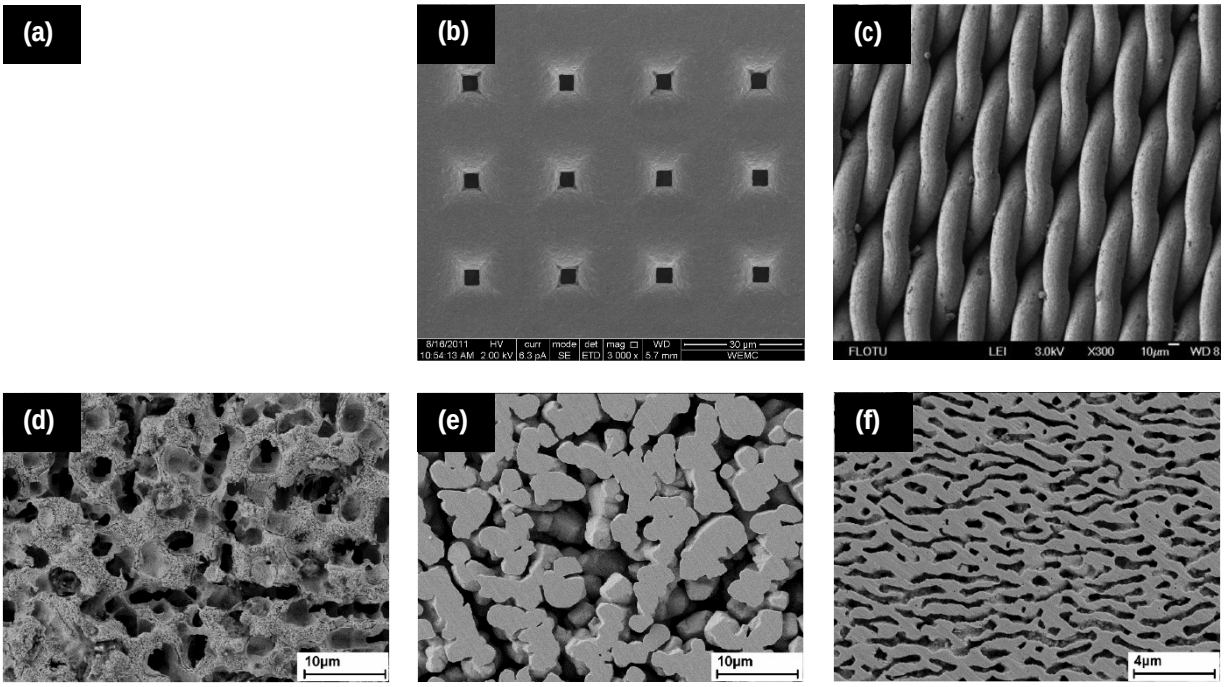

Fig. 7. SEM images of metallic membranes used in PME: (a,b) Nickel microsieve with rectangular (pore size: ~13×337 μm, porosity: 4.79%) and squared pores (pore size: 4×4 μm, porosity: 2.65%), respectively [62], (c) woven stainless steel mesh membrane (pore size: 2 μm) [29], and (d,e, and f) LF-γ (pore size: 700-900 nm, porosity: 51%), LF-γ' (pore size: ~200 nm, porosity: 41%) and TM-γ' (pore size: ~300 nm, porosity: 26%) nickel superalloy membranes [63]. LF and TM represent thermally (load-free) and thermo-mechanically coarsened membranes, respectively, while γ and γ' represent the nickel-rich and nickel aluminide phases, respectively, which is subsequently separated from the matrix through electrochemical phase extraction.

The first detailed study on PME using nickel microsieves was reported by Nazir et al [62, 64]. The authors used nickel microsieves (Veco B.V., The Netherlands) having rectangular pores with a high aspect ratio of around 30: the pore width was in the range of 7-13 μm, while pore length was around 300-400 μm. These microsieves are produced by plating or photo defined electroforming, a process specialized for the manufacturing of high precision metal parts through atom-by-atom deposition. It is a cost-effective technique providing extreme accuracy, which can produce highly porous sieves with homogenous pore size distribution. Under the tested process conditions, droplet size and span for the prepared O/W emulsion was in the range of 5-10 μm (always less than the smallest pore dimension, i.e., pore width) and 1-1.5, respectively. It should be noted that microsieves with such a high pore aspect ratio are not suitable for DME (which typically requires slit-like pores with an aspect ratio between 3 and 5) and can only be used in PME. On comparison with a nickel membrane having squared pores (4×4 μm), it was established that the shortest pore dimension (i.e., pore width) of elongated pores was responsible for droplet breakup, while

extended pore length permitted much higher production rates and a less chance of fouling. The droplet disruption in rectangular pores was governed by interfacial and inertial forces, so a smaller droplet size was achieved at higher pore Reynolds number (discussed in more detail in Section 4).

Santos et al [65] prepared O/W emulsions using micro-engineering nickel membranes having circular pores of 10 and 20 μm diameter. The mean median droplet size after the second pass was less than the respective pore size when the transmembrane flux was typically more than 500 $L \cdot m^{-2} \cdot h^{-1}$. However, the droplet size distribution was broader with a bimodal distribution for 10 μm membrane that was correlated to an intensive (but incomplete) droplet breakup. Contrary to this, a unimodal distribution was observed with nickel microsieves having rectangular pores, due to an intense and complete droplet break up [62].

Kohnke et al [63] used lab-made nickel-based nanoporous superalloy membranes for the preparation of nanoemulsions. The fabrication of these membranes starts by first developing an interpenetrating network of γ-matrix phase (a nickel-rich solid solution) and γ'-precipitates (Ni_3Al) through thermo-mechanical (TM) or thermal (load-free, LF) treatments. Subsequently, either γ or γ'-phase is separated from the matrix through electrochemical phase extraction. It results in the formation of nanoporous membranes having channel-like or interconnected pores, depending upon different thermo-mechanical conditions applied during the fabrication process (Fig. 7). Apart from high thermal and mechanical strength, these membranes were claimed to possess high chemical stability, thus making them suitable for longer operating times. These membranes successfully produced nanoemulsions (average droplet size: ~150 nm) with acceptable particle size distributions comparable to commonly used track-etched polyester membranes.

The stainless steel is another commonly used material for the fabrication of micro-/nanoporous metallic membranes [26]. The stainless-steel membranes are exceptionally durable and can tolerate extreme operating conditions (i.e., pH, temperature and pressure). The woven mesh and laser drilled type stainless steel membranes were used by several groups for the preparation of O/W and W/O emulsions through DME [66, 67]. However, to our knowledge, there is only one study reporting PME using stainless steel (woven type) membranes having pore size of 1-2 μm [29]. The polystyrene nanospheres in the range of 40-120 nm with 15% coefficient of variation (CV) were produced by combining PME and thermally initiated mini-emulsion polymerization process.

3.4. Unconsolidated porous media (dynamic membranes)

In PME, the coarse emulsion passes through the membrane as a whole, which makes membrane susceptible to depth fouling, especially when biopolymers (like proteins) are used as emulsifiers. This is so far a major drawback associated to PME using conventional membranes with tortuous pore structure. A vigorous cleaning of the membrane is often required after each emulsification cycle; nevertheless, the membrane pores are usually inaccessible to cleaning agents in case of a tortuous pore structure, and also not all the membranes can tolerate cleaning agents. In this regard, microengineered membranes with straight-through pores could perform well but they can achieve limited droplet disruption. An alternative approach is the use of unconsolidated porous media (dynamic membranes) of suitable solid particles, as the apparatus can be cleaned easily by resuspending solid particles during the cleaning process. Van der Zwan et al [19] introduced such system in which glass microbeads were used to produce O/W emulsions through PME. The same research group continued working on the packed bed system and came up with a more detailed study by considering different process and formulation conditions [68, 69]. The reported average droplet size for O/W emulsion was less than 5 μm (droplet to pore size ratio: ~0.2) with a narrow droplet size distribution (droplet span: ~0.75). This represents a very simple and inexpensive approach wherein packed bed of different interstitial voids and thicknesses can be easily established to achieve desirable hydrodynamic conditions. The packed bed system has found useful applications in the production of protein stabilized emulsions [70], double emulsions [71, 72], microcapsules [73], and foams [74]. The future research in this field could focus on particles of different materials and shapes, to construct packed bed of different properties.

3.5. Disposable filters

PME is a robust system that can handle variable volumes of the feed emulsion. The systems that are presented above are usually suitable to handle large volumes in a continuous operation. However, if tiny emulsion volumes are to be processed, as little as 1 ml, disposable syringe filters can be used to extrude emulsions in a syringe, either manually (e.g., commercial Liposofast extruders) [49] or through an externally applied pressure [33]. Apart from PME's inherent simplicity, the possibility to use disposable materials and the ability to handle small emulsion volumes make PME very suitable to handle highly potent and toxic substances and to prevent cross-contamination of prepared emulsions [75]. Various types of syringe filters composed of borosilicate glass fibers, polyethersulfone,

nylon, cellulose acetate and cellulose ester have been applied in PME for the preparation of single and double emulsions, nanoemulsions, and microparticles [75-79].

4. Theoretical aspects of droplet disruption in PME

As PME is a pressure driven process, a pressure drop is always required to push coarse emulsion through a membrane, usually for a certain number of cycles (*N*) until small and uniform droplets are obtained. The applied pressure should always be higher than a certain threshold value, which is termed as critical pressure or capillary pressure, ΔP_{cr}. The critical pressure depends on interfacial tension, γ, between the two immiscible liquid phases, pore size, d_p, and initial droplet size, d_d. Park et al [23] derived an equation for ΔP_{cr} assuming that droplets larger than the pores have an ellipsoidal shape when they pass through a membrane:

$$\Delta P_{cr} = \text{[illegible]} \quad (1)$$

where, ξ is the ratio between initial droplet size and pore size, i.e., d_d / d_p. The similar equation was proposed by Nazzal and Wiesner [80]. For droplets much larger than the pores (i.e., ξ >> 1), the critical pressure is:

$$\Delta P_{cr} = \frac{4\gamma \cos\theta}{d_p} \quad (2)$$

where, θ is the contact angle between membrane surface and dispersed phase. The transmembrane pressure, ΔP, usually 10-50 times larger than ΔP_{cr} [18], is the main driving force for the droplet disruption in PME. In the absence of droplet disruption and membrane fouling, ΔP is directly proportional to the transmembrane flux, J, through Darcy's law:

$$\Delta P = J\eta R_m \quad (3)$$

where, η is emulsion viscosity, and R_m is membrane resistance. However, part of the applied mechanical energy (transmembrane pressure) is utilized for droplet deformation and disruption (ΔP_{def}) and to overcome fouling (internal and external) resistance (ΔP_{foul}), and an extended form of Eq. (3) is more appropriate [18]:

$$\Delta P = \underbrace{J_i \eta (R_m + R_{f,i})}_{\Delta P_{foul}} + \underbrace{k \phi \gamma \, \text{[illegible]}}_{\Delta P_{def}} \quad (4)$$

where, k is a constant, ϕ is dispersed phase volume fraction, and J_i, $d_{d,i}$ and $R_{f,i}$ are the transmembrane flux, final droplet diameter, and overall fouling resistance of the i^{th} pass through the membrane, respectively. It should be

noted that the local pressure drop along a pore varies with the variation of capillary pressure, which reflects the evolution of interfacial curvature and interfacial tension [81]. Alliod et al [82] pointed out that the pressure drop along the pipes leading from high pressure pump to membrane module may not be negligible compared to ΔP_{cap} and ΔP_{tm}, especially at high flow rates and emulsion viscosities. Therefore, under such conditions, another pressure term (i.e., ΔP_{pipe}) should be added to the right-hand side of Eq. (4).

The transmembrane pressure and the membrane properties are the main factors that determine the final droplet size of the resulting emulsion. The prevailing hydrodynamic conditions result in generation of shear stress at pore walls, τ_w, that can be defined for cylindrical pores as [18]:

$$\tau_w = \frac{\xi J \eta}{\varepsilon d_p} \quad (5)$$

where, ε and ξ are porosity and pore tortuosity of the membrane, respectively. According to Eq. (5), internal shear stress can be maximized by increasing transmembrane flux and emulsion viscosity, and by decreasing pore size, which will lead to smaller droplets. Moreover, for a constant energy input, there is usually a linear relation between final droplet size and membrane pore size, i.e., $d_d = c\,d_p$ [11]. In the preparation of microemulsions, $c << 0.5$ even at low pressures due to self-emulsification, while in case of nanoemulsions and macroemulsions, c is typically around 0.7-1.5 [83-85]. Nevertheless, $c < 0.5$ is still achievable for nanoemulsions but under specific conditions (i.e., high ΔP and suitable membrane properties), as can be seen from the data presented in Table A.1.

The mechanisms of droplet breakup in membrane pores are highly complicated and can be best understood by direct visual insight. In an early study, van der Zwan et al [86] microscopically visualized the droplet breakup in PME using a transparent chip with stacked layers of rectangular obstacles that mimic a membrane with tortuous branched pores (Fig. 8). At constant pressure difference, the most uniform droplets were formed at an intermediate membrane thickness that provided an optimum balance between sufficient number of constrictions and sufficiently high flow rate inside constrictions [86].

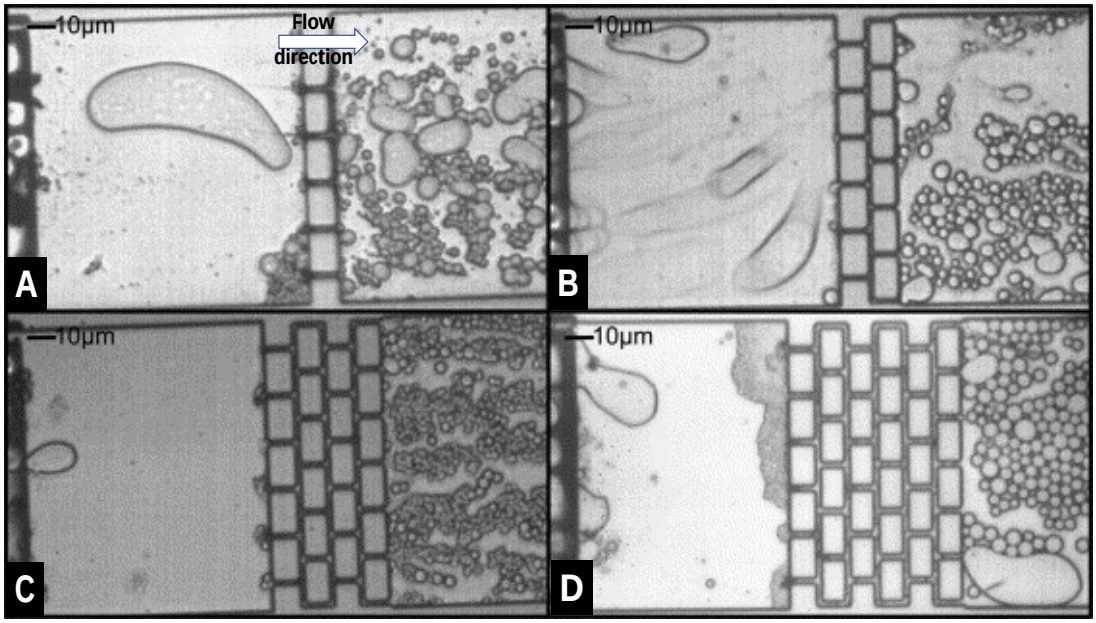

Fig. 8. Droplet break-up resulting from a pass through (A) one layer, (B) two layers, (C) four layers, and (D) six layers of stacked rectangular obstacles. Channels depth: 2 μm; channel width in the brick structure: 2 μm.

Thee major mechanisms responsible for droplet breakup found by direct visual observation are [86]: *i*) snap-off due to localized shear forces at a pore branching similar to droplet break-up mechanism in T-junctions, *ii*) interfacial tension effects like Rayleigh and Laplace instabilities, and *iii*) steric hindrance between droplets augmented due to accumulation of droplets on the membrane surface and inside the channels. This study provided a fundamental insight into droplet breakup in PME; however, due to a great variety of the porous media used for PME, the droplet breakup cannot be fully explained by these three mechanisms. The magnitude of each force depends on a specific membrane and the prevailing flow conditions. For instance, droplet breakup in straight-through pores (e.g., nickel microsieve) and interconnected pores (e.g., SPG membrane) is entirely different, and even within the same pore geometry a different droplet breakup may operate under different hydrodynamic conditions. Therefore, type and extent of each droplet disruption force and droplet breakup mechanism may vary for different PME systems, which makes it difficult to develop a generalized model to predict final droplet size. Some researchers developed empirical scaling relations for their PME systems, and used an energy density, E_V, approach to estimate final droplet size. The energy density can be related to transmembrane pressure as:

$$E_V = \frac{V}{t} = \frac{J_w t}{t} = J_w \qquad (6)$$

where, P is power input, and $\dot{V}$ is volumetric flow rate of emulsion. For more than one pass (as it usually happens in PME), specific energy densities of all the passes should be summed up [19]. The energy density approach (Eq. 6) was used for the first time by Karbstein and Schubert [87] for conventional continuous mechanical emulsification processes, and it was found helpful to develop scaling relations for some PME processes (Table 1). The optimum energy density for generating uniformly-sized droplets decreases with increasing pore size [88]. Due to low energy densities applied during droplet breakup (around 10^5-10^6 J/m^3 for SPG membrane having pore size between 1-10 μm), PME is characterized with high encapsulation efficiency of active ingredients entrapped within emulsion droplets [89, 90] and with high internal porosity of particles generated from double emulsion droplets by PME combined with solvent evaporation [91].

Table 1. Scaling relations based on energy density approach.

Scaling relation		Description	Ref.
$d_{3,2} = C E_v^{-b}$	(7)	The basic expression used to relate droplet size with energy density for conventional emulsification devices.	[87]
$d_{3,2} = C E_v^{-b} N^{-a}$	(8)	A modified expression that can be applied for PME with multiple extrusions through a membrane.	[19, 64]
$\frac{d_{3,2}}{d_p} = C E_v^{-b} \left(\frac{H_b}{D_b}\right)^{a} \left(\frac{\eta_d}{\eta_c}\right)^{\beta}$	(9)	A modified expression for the packed bed system to relate the droplet size with a pore size, process parameters and viscosity ratio.	[69]

Where, E_v = energy density; $d_{3,2}$ = Sauter mean droplet diameter; d_p = pore diameter; H_b/D_b = height to diameter ratio of the packed bed (dynamic membrane); η_d/η_c = viscosity ratio of the dispersed and continuous phases; N = number of passes through the membrane; C, a, b, and β = parameters whose numerical values depend on the type of the PME system (Table A.2).

Apart from the energy density approach, various dimensionless numbers have been used to explain flow behavior and droplet breakup mechanism in PME (Table 2). Nazir et al [68] characterized the droplet breakup mechanism as a function of Reynolds number, Re, in packed bed PME for different interstitial voids, d_p, and heights, H_b, of the packed bed (d_p and H_b are analogous to membrane pore size and thickness), as shown in Fig. 9. At low Reynolds number, both data points (i.e., for variables d_p and H_b) are well separated from each other, but then merged at Re > 40. This can be explained by different droplet breakup mechanisms prevailing at low and high Reynolds numbers. At low Reynolds number, the droplet breakup is dominated by spontaneous droplet snap-off and hence the constriction effect is more pronounced leading to a narrow droplet size distribution (Fig. 9b). The droplet snap-off mainly occurs at pore inlets, pore outlets and pore junctions, due to localized shear and pressure forces that are analogous to those in microfluidic junctions and flow focusing channels [92]. Moreover, the interfacial forces such as Laplace and Rayleigh instabilities can also be accounted for droplet disruption inside the pores. The Laplace pressure differences usually originate within a deformed droplet while passing through a constriction, leading to

droplet breakup, which is similar to the droplet generation mechanism in step microfluidic emulsification [93]. On the other hand, Rayleigh instability operates on an elongated droplet inside a pore at high flow rates, when the droplet is separated from the pore wall via a lubrication layer of continuous phase [94, 95]. The merging of two curves in Fig. 9a at higher Reynolds number (i.e., at low Re_d or high Re_p) indicates a change in the droplet breakup mechanism, which is dominated by interfacial and inertial effects. The thickness of the lubrication layer increases at higher Reynolds number, which results in a decrease in radius, r_d, of the oil cylinders. These elongated droplets ultimately break into smaller droplets when $2\pi r_d < \lambda$, where λ is the Rayleigh-Plateau length. The thickness of lubrication layer is directly proportional to $Re_p(\mu_c u / \sigma)^{2/3}$ [94], where μ_c is continuous phase viscosity, u is droplet velocity inside the pores ($u \approx Ca$), and σ is interfacial tension. Thus, apart from high Reynolds number, a high viscosity of continuous phase also promotes droplet disruption by increasing the thickness of lubrication layer. The effect of dispersed to continuous-phase viscosity ratio (μ_d / μ_c) on final droplet size is also shown in Eq. 9 [69], in which the term $(\mu_d / \mu_c)^{\zeta}$ becomes relevant only at high continuous phase viscosity (Table A.2). A relatively wider droplet size distribution in Fig. 9b for $Ca > 40$, can be explained as the formation of small satellite droplets due to interfacial instabilities, which further supports the existence of different droplet breakup regimes as a function of Reynolds number. Satellite droplets are predominantly formed at high shear stresses due to multiple break-up locations along the droplet neck [96].

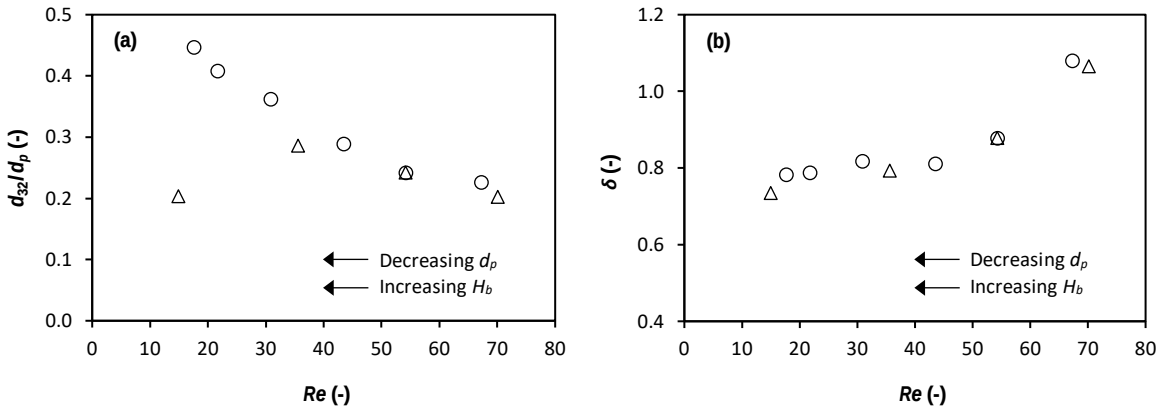

Fig 9. (a) Dimensionless droplet diameter, Ω_{d}/Ω_{p}, and (b) droplet size span, δ, after five passes through a porous bed, as a function of Reynolds number, Re: (Δ) variable pore size, d_p, and (O) variable bed height, H_b [68]. The emulsion consisted of 5% hexadecane dispersed in 0.5% Tween 20 aqueous solution. The applied pressure was constant at 200 kPa.

Horning and Fritsching [97] used membranes consisting of spherical or non-spherical sintered glass particles and expressed the mean Sauter diameter (Ω_{d}) of droplets in product emulsion and the droplet disruption coefficient achieved in PME (ψ = a ratio of initial to final droplet diameter) in terms of Re and structural properties of membrane (i.e., pore size, Ω_{p}, porosity, -, and pore tortuosity, ,), as:

$$\psi = \alpha_{1} \cdot Re^{\beta_{1}} \cdot \Omega_{p}^{\gamma_{1}} \cdot \varepsilon^{\delta_{1}} \cdot \tau^{\eta_{1}} \quad (10)$$

$$\Omega_{d} = \alpha_{2} \cdot Re^{\beta_{2}} \cdot \Omega_{p}^{\gamma_{2}} \cdot \varepsilon^{\delta_{2}} \cdot \tau^{\eta_{2}} \quad (11)$$

The values for the best-fit coefficients in Eqs. (10) and (11) are presented in Table A.3. For both shapes of sintered particles (i.e., spherical and non-spherical), Reynolds number and pore size showed a higher impact on ψ and final Ω_{d} than membrane porosity and tortuosity. The minimum Ω_{d} of a Tween 20 stabilized rapeseed oil-in-water emulsion was 9 μm at 0.5 MPa using non-spherical particulate membrane structure with the median pore size of 13 μm. The higher membrane porosity led to higher ψ, as pore size decreased with increasing porosity for all the membranes used in this study. For the spherical particulate membranes, higher pore tortuosity resulted in higher liquid dispersion. Higher pore tortuosity is expected to increase residence time of droplets moving through the porous system. Therefore, the probability of reaching maximum dispersion while passing through a pore with minimum diameter is increased.

Table 2. Dimensionless numbers used in PME studies to characterize flow behavior and droplet breakup process.

Dimensionless number	General expression	Description	Ref.
Reynolds number	$Re = \frac{\rho_c v d_p}{\eta_c}$ (12)	A ratio of inertial to viscous forces in pores. Usually, pore-based Reynolds number is used in PME studies to characterize the flow properties.	[68, 97]
Weber number	$We = \frac{\rho_c v^2 d_d}{\sigma}$ (13)	A ratio of inertial to interfacial forces acting on a droplet, which is normally used to identify stable and unstable or disrupting droplet regime.	[62, 98]
Capillary number	$Ca = \frac{\eta_c v}{\sigma}$ (14a) $Ca = \frac{\eta_c \dot{\gamma} d_d}{\sigma}$ (14b) $Ca = \frac{\eta_c v}{\sigma}\left(\frac{d_d}{d_p}\right)$ (14c)	A ratio of viscous to interfacial forces; or alternatively, a ratio between We and Re. The capillary number can be expressed in terms of pore velocity (Eqs. 14a and 14c) or shear rate (Eq. 14b); and is commonly used to describe droplet disruption as function of shear. Eq. (14c) is a modified capillary number used by Navarro et al [99].	[86, 98, 99]
Ohnesorge number	$Oh = \frac{\sqrt{We}}{Re} = \frac{\eta_c}{\sqrt{\rho_c \sigma d_d}}$ (15a) $Oh^* = \frac{\sqrt{\eta_d \eta_c}}{\sqrt{\rho_c \sigma d_d}}$ (15b)	Ohnesorge number relates all the major forces (i.e., inertial, viscous, interfacial) involved in droplet disruption. Oh^* is a modified Ohnesorge number used by Güell et al [100].	[100]
Pressure ratio	$\acute{P} = \frac{\Delta P_{tm} d_d}{\sigma}$ (16)	A ratio of transmembrane pressure to the droplet Laplace pressure, which relates the applied energy to the minimum amount of energy needed to deform the droplet.	[64]

Where, ρ_c = continuous phase (or emulsion) density, η_c = continuous phase (or emulsion) viscosity, η_d = dispersed phase viscosity, σ = interfacial tension, v = pore velocity, d_d = droplet diameter (usually Sauter mean diameter), d_p = pore diameter, δ_m = membrane thickness, $\dot{\gamma}$ = shear rate (v/d_p), ΔP_{tm} = transmembrane pressure. The outgoing (final) droplet diameter is used in We, Oh, and Oh^*, while ingoing (initial) droplet diameter is used in all other dimensionless numbers.

In case of PME via straight-through pores (such as in microengineered metallic membranes), shear inside the pore is less relevant to droplet breakup than in membranes with interconnected tortuous pores. The droplets are elongated after passing through constrictions and are then broken down on downstream side of the membrane due to external shear forces and sudden change in flow geometry. This was reported by Nazir et al [62] for droplet breakup in nickel microsieves having rectangular and square pores. The droplet breakup mechanism was described by plotting Weber number, We, against dimensionless pressure, $\acute{P}$, which is a ratio between the applied pressure and droplet Laplace pressure (Fig. 10). At constant applied pressure, the microsieves with rectangular pores having smallest pore width (7.1×413 μm) performed better (i.e., higher flow rate and smaller droplet size) than the microsieves with square pores (4×4 μm) and rectangular pores having greater pore width. As shown in Fig. 10, at the start of emulsification cycle (i.e., at high $\acute{P}$ value), Weber number was highest for microsieve with the narrowest rectangular pores. This can be linked to a high potential of such pore geometry for an efficient droplet disruption. This can be explained as, an incoming droplet is effectively elongated while passing through a narrow slit (as a result of high aspect ratio of pore and high flow velocities), which ultimately leads to their breakage into smaller droplets due to interfacial instabilities. With decreasing droplet size that usually occurs with repetitive emulsification cycles,

Weber number is reduced, which can be linked to a reduction in droplet breakup potential (i.e., the emulsification process is approaching its limit). The same is also true for the emulsification runs carried out at low transmembrane pressure (i.e., low flow velocity), which also leads to a lower Weber number, resulting in a lower droplet breakup potential. This explanation of droplet breakup in straight-through rectangular pores was further validated by Kaade et al [101, 102] who used hydrophobic nickel microsieves (contact angle: 115°) having rectangular pores (5×300 μm) for the preparation of lemon oil-in-water emulsions. Interestingly, even the hydrophobic surface resulted in successful O/W emulsification, which contradicts the principle of a typical PME process that demands a hydrophilic membrane for O/W emulsion. In fact, at high flow rates in straight-through pores (especially in case of rectangular pores), the membrane wettability is expected to have less detrimental impact on emulsification results. The researchers also reported a change in wettability of the membrane (a decrease in contact angle) due to repetitive emulsification and cleaning cycles. The change in membrane wettability may occur due to surface interactions between the membrane and the surface-active components present in the processed emulsion [103].

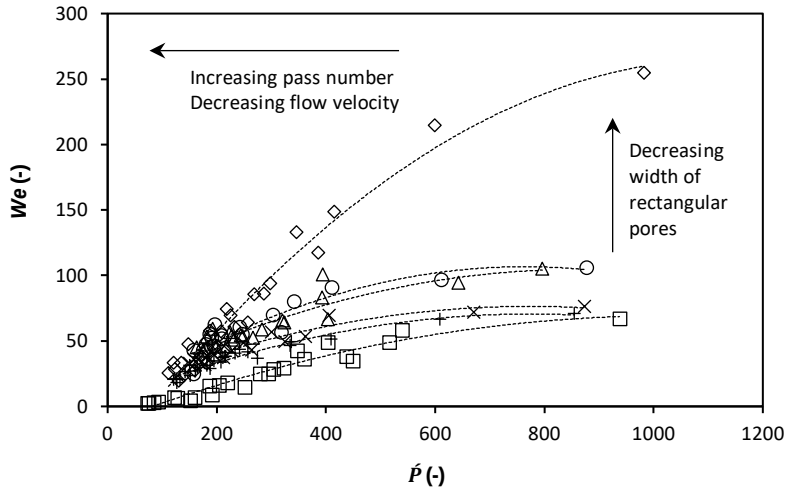

Fig. 10. Weber number, $\dot{\omega}\mathbb{Q}$, as a function of pressure ratio, $\acute{P}$, for the preparation of O/W emulsion using nickel microsieves having square and rectangular pores: (□) 4×4 μm, (◊) 7.1×413 μm, (○) 10.6×330 μm, (Δ) 11.6×331 μm, (×) 12.8×329 μm and (+) 13.2×337 μm microsieves. [62]. The emulsion consisted of 5% hexadecane dispersed in 0.5% Tween 20 aqueous solution. The applied pressure ranged between 0.3 bar and 2 bar, while the number of passes through the membrane was between 1 and 5.

Güell et al [100] suggested using Ohnesorge number, which relates viscous forces to inertial and interfacial forces, to describe a PME process in non-dimensional form. They defined a modified Ohnesorge number, $\ddot{\upsilon}\mathbb{Q}^{z}$ (Eq. 15b) in which membrane thickness and pore diameter were incorporated in the denominator, and final droplet size in

the numerator. They used a flat polymeric membrane to produce hexadecane-in-water emulsions stabilized with bovine serum albumin (BSA), whey protein and Tween 20 of various concentrations. The droplet disruption ($\dot{\varphi}$ = a ratio of initial to final $\Omega_{d,p}$) was higher at high flux, whatever the emulsifier was used; nevertheless, superior droplet disruption was achieved with Tween 20 at or above critical micelle concentration (Fig. 11a). When the modified Ohnesorge number, $\breve{\upsilon}\Omega^{z}$, was calculated using the apparent (dynamic) interfacial tension and plotted against the pressure ratio, data points for all all surfactants were roughly lined up along a master line with a negative slope, as shown in Fig. 11b. A smaller $\breve{\upsilon}\Omega^{z}$ value corresponds to greater droplet size reduction achieved at higher ratio of applied pressure to Laplace pressure of the feed droplet.

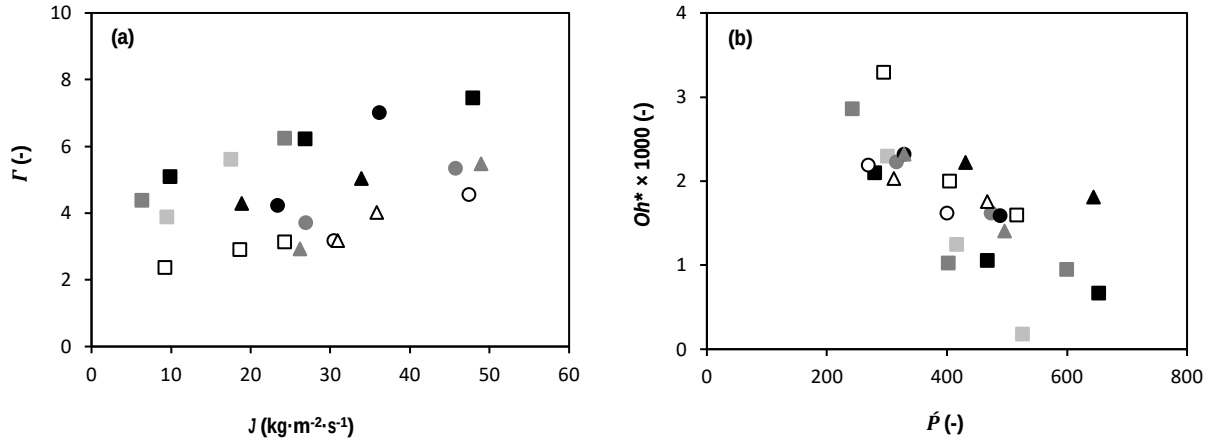

Fig. 11. (a) Droplet disruption, $\dot{\varphi}$, as a function of transmembrane flux, $\dot{\upsilon}$, and (b) modified Ohnesorge number, $\breve{\upsilon}\Omega^{z}$, as a function of pressure ratio, $\acute{P}$, for O/W emulsions prepared using different concentrations of Tween 20 [(□) 0.1%, (■) 0.5%, (■) 1.25%, and (■) 2%], bovine serum albumin (BSA) [(○) 0.25%, (●) 0.5%, and (●) 1%], and whey protein [( ) 0.25%, (▲) 0.5%, and (▲) 1%]. The dispersed phase was pure hexadecane, the dispersed phase content was 10%, and the membrane used was nitrocellulose mixed ester (pore size: 0.8 μm, thickness: 150 μm, porosity: 80%) [100].

5. Breakup of a single drop in idealized pore geometries

The breakup of a single drop in various idealized pore geometries has been investigated numerically and experimentally, which provides a useful insight into the fundamental aspects of droplet breakup in PME. However, much remains to be done to apply the results from these fundamental studies to the design of new membranes for PME [104]. When a droplet encounters a pore opening, it faces one of the following four fates: rejection, pinning (attachment), permeation, or breakup [105]. The droplet fate depends on the size of droplet and pore opening, flow velocity in the pore, pore geometry and physical properties of the droplet phase and surrounding fluid. Wollborn et al [98] analyzed deformation and breakup of a single drop larger than the pore size ($\Omega_{j}/\Omega_{ص}$ = 2.25-2.75) in straight-

through cylindrical pores at variable capillary number, $\acute{o}\acute{\omega}$ (Fig. 12). The interfacial stress distribution was calculated through computational fluid dynamic (CFD) simulations based on volume-of-fluid method, and the results were validated experimentally by microscopic investigations of droplet deformation in a glass tube. The liquid-liquid interfacial stresses were primarily responsible for droplet deformation, even when the pore-wall interfacial stresses were an order of magnitude higher. The initial droplet size barely influenced the interfacial stresses but affected the droplet deformation through pressure drop in the pore. At lowest capillary number, droplet flows in perfect plug flow while being in direct contact with the pore wall over the whole length. As capillary number increases, the contact area between the moving droplet and the pore wall was reduced, which allowed for more liquid-liquid interactions. As a result, the regions of low interfacial stresses started to develop at the tip of droplet (blue parts). This led to an increase in velocity of the detached portion of droplet as compared to the part that was still attached to the wall. As time progressed, it resulted in further constriction and elongation of the detached part. At the highest capillary number ($\acute{o}\acute{\omega}$ = 0.365), a lip was formed at the bottom of the droplet due to local instabilities, which eventually caused the droplet breakup.

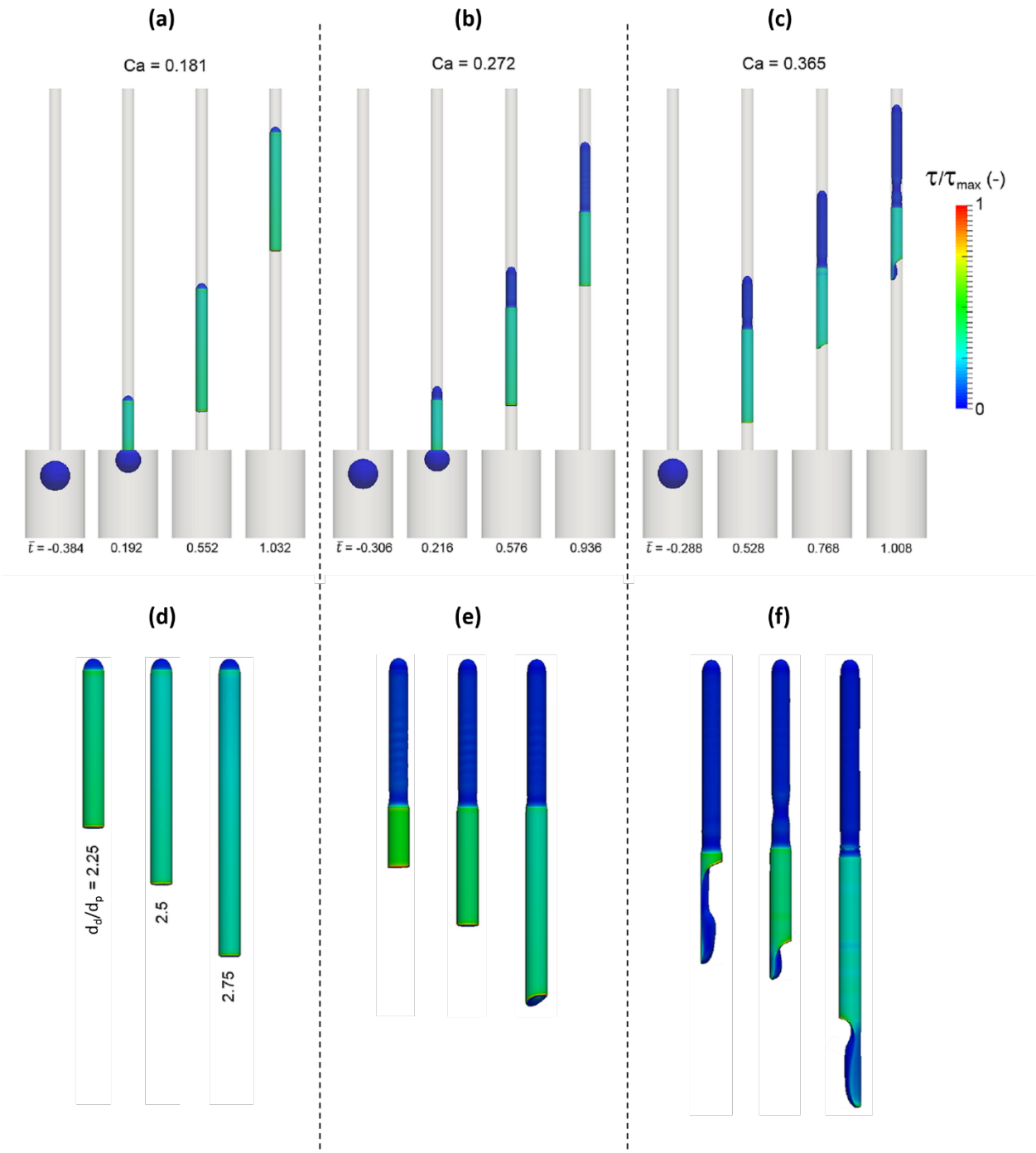

Fig. 12. (a-c) Simulation of a single droplet movement at Ω_z/Ω_d = 2.5 in a 200 µm pore for different capillary numbers, $\delta\omega$, and dimensionless times, $\bar{t}=t v_{in}/\Omega_d$, where t is the actual time and v_{in} is the inlet velocity). (d-f) Simulation of droplet deformation in a 200 µm pore for three different Ω_z/Ω_d and $\delta\omega$ values at similar positions close to the pore outlet. The dispersed phase was medium chain triglycerides (viscosity: 0.029 Pa·s, density: 952 kg·m^{-3}) and the continuous phase was pure water (viscosity: 1 mPa·s, density: 1000 kg·m^{-3}). The interfacial tension was 0.024 N·m^{-1}. The colouring indicates the shear at the droplet interface relative to the maximum shear, τ/τ_{max}. The maximum shear is located at the trailing edge of the droplet which is in contact with the pore wall [98].

Earlier, Link et al [106] found that droplet plugs never break in straight channels even if they are longer than Rayleigh-Plateau limit, because of the nearby walls that act to suppress growth of instabilities. Once droplets reach a pore junction, for example a T-junction, they are subjected to extensional stresses at the stagnation point, which are much larger than the shear stresses upstream of the junction. For any ratio of the initial droplet length to the pore width, there is a critical flow rate above which the droplets will break into two daughter droplets. Sufficiently large droplets always break at T-junction independent of the flow rate. On the other hand, smaller droplets do not break if they are travelling too slowly down a pore, emphasizing the importance of transmembrane flux as a key driving force of the droplet breakup.

Droplet breakup is more effective in the presence of obstacles in pores than in non-obstructed pores, but the break-up probability highly depends on the inlet velocity. When a drop, which is large compared to the pore width and more viscous than the continuous phase, meets an obstacle partially blocking a pore, there is a critical speed above which the drop breaks into two smaller drops and below which all of the droplet fluid bypasses the obstacle on one side only without breakup [107]. The non-dimensional drop speed, defined as a capillary number ($Ca = \mu_c v_c / A\sigma$, where v_c is the continuous phase flow rate, and A is the free cross-sectional area of the pore), can be used to predict whether or not a drop will break into two daughter droplets. At capillary numbers below a critical value, i.e., $Ca < Ca_{crit}$, drops do not break after collision with an obstacle despite significant deformation, while at $Ca > Ca_{crit}$ drops break. The critical capillary number depends also on the size of mother droplets and the size and geometry of obstacles, as shown in Fig. 13. Small droplets in Fig. 13(a) flow through multiple linear arrays of square obstacles without breaking up. However, larger droplets are more unstable and break into daughter droplets. The break-up probability depends on local flow and pressure distributions, leading to creation of polydispersed daughter droplets.

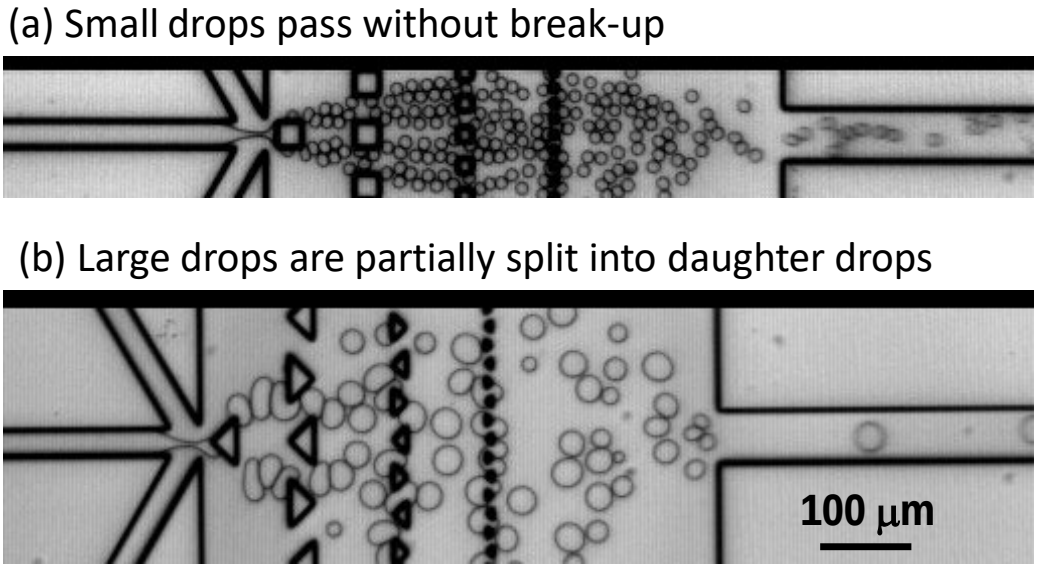

Fig. 13. Obstacle-mediated droplet generation and splitting: (a) small droplets formed at 3000 Hz pass through multiple arrays of square obstacles without breaking up; (b) large droplets partially break into smaller droplets due to more extensive deformation. The dispersed phase is soybean oil and the continuous phase is an aqueous 1% SDS solution [108]. The videos of droplet break-up shown in the supplement are provided by courtesy of Prof. Mitsutoshi Nakajima from Tsukuba University, Japan.

Navarro et al [99] used a boundary-integral algorithm to simulate behavior of droplets when they move through narrow pores and predict whether droplets will break into smaller drops or not. At the investigated drop diameter to pore length ratio, Ω, of 0.2-0.8, the drops did break due to interactions with pore walls (direct breaking) or due to drop stretching and capillary pinch-off (indirect breaking). Smaller drops with high viscosities at low capillary numbers were more likely to go through the pores without breaking. Relatively large drops with η_j / η_r = 1 and Ω = 0.8 break in pores with a Y-bifurcation for all capillary numbers examined (Ca = 0.16-0.48), which is similar to what was found by Link et al [106] for the T-bifurcation and plug flow. Pore geometry was found to have a strong effect on droplet breakup, with no breakup observed in pores with a circular constriction (because a rounded shape of the constriction caused small elongation and allowed the drop to regain its spherical shape after exiting the constriction). Drop breakup was more effective in the pores with an H-constriction, especially for increased pore lengths (Fig. 14). This type of pore geometry occurs in thin membranes with straight-through pores such as track-etched, laser drilled, and etched pores. The studies in channels with diffuser/nozzle structures have shown that the liquid-liquid interface turns into a saddle shape in constriction, and this shape makes droplet prone to breakup once

it comes out of the constriction [109]. The critical droplet break-up flow rate mainly depends on ratio of the hydrodynamic diameters of constriction and downstream channel [110]. Pore networks with bifurcations (similar to pores in SPG membrane, sintered glass and ceramic filters) provided more effective drop breakup than the pores with constrictions, but no obstacle or bifurcation [99].

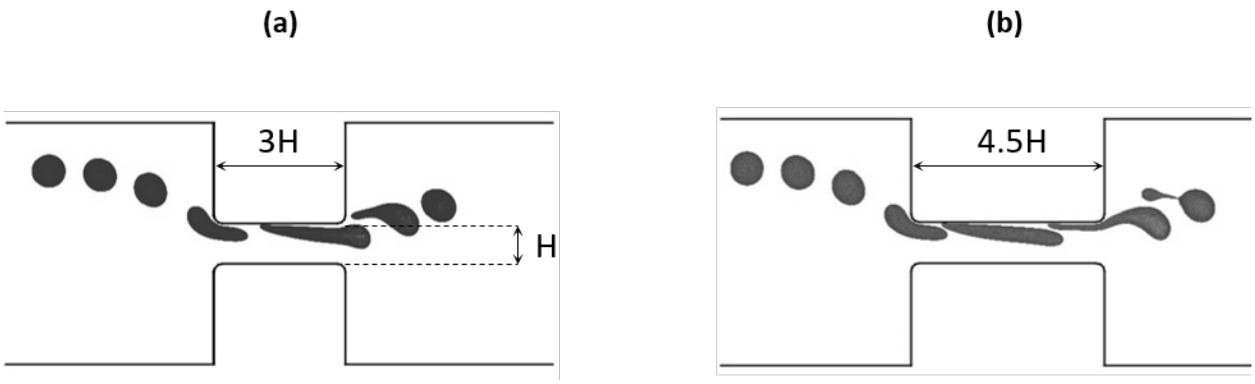

Fig. 14. Snapshots of the trajectories of a single drop with $\eta_ژ / \eta_ڔ$ = 1, ῾Ω = 0.8, and ὅῴ = 0.32, while passing through a pore with an H-constriction of height, ῎Ο (῎Ο is analogous to pore diameter, ῾Ω$_ڡ$): (a) the droplet passes through the constriction without breaking when the constriction length is 3῎Ο, (b) the droplet breaks up when the constriction length is 4.5῎Ο. Here, $\eta_ژ / \eta_ڔ$ is the dispersed to continuous-phase viscosity ratio, ῾Ω is the drop size to constriction length ratio, and ὅῴ is the modified capillary number calculated using Eq. (14c) [99].

6. Membrane fouling in PME

The membranes in PME are prone to fouling that reduces production rate and might affect droplet breakup due to altered membrane porosity and wettability. The type and extent of fouling depend on membrane properties, process conditions, and feed formulation. In a symmetric membrane with interconnected pores, surface as well as depth fouling of the membrane (due to pore blockage with emulsion droplets) can be expected. The presence of electrostatic or hydrophobic interactions may further worsen the situation. The mean droplet size and the dispersed phase fraction in the emulsion passing through the membrane affect the flow resistance, as shown by Eq. (4). For repetitive passage of emulsion through the membrane, the maximum flow resistance occurs in the first pass (as the applied energy is mainly used for droplet disruption), leading to low transmembrane flux and accumulation of droplets on the membrane surface and within pores. In the subsequent extrusions, an increase in transmembrane flux may be expected at constant pressure due to a decrease in droplet size [111]. However, this is not always true as congestion of membrane pores may also occur by small droplets, especially at higher droplet concentration [64]. Contrary to pore blockage by emulsion droplets (which is usually reversible), the presence of macromolecules

(proteins and polysaccharides) in the continuous phase can lead to a severe form of irreversible fouling, the extent of which depends on the type and concentration of macromolecules and membrane properties.

The cleaning protocols depend upon the membrane nature as well as on the type and degree of fouling. The efficiency of the cleaning process can be estimated by comparing water fluxes of cleaned and virgin membranes at the same pressure and temperature [112], by visualizing the membrane surface before and after cleaning using surface characterization techniques such as scanning electron microscopy (SEM), attenuated total reflectance infrared microspectroscopy (ATR-IRMS), atomic force microscopy (AFM), energy dispersive X-ray spectroscopy (EDS), and nuclear magnetic resonance (NMR) [113], or by assessing the performance of a cleaned membrane in PME [114]. The flux can be recovered near to its original value for a pre-fouled membrane by implementing a suitable cleaning procedure. For instance, successful cleaning of SPG membrane was reported by dipping the membrane first in ethanol and then in toluene for few days. Afterwards, the membrane was heated in a muffle furnace at 500°C for half an hour [18]. The method was found efficient even when proteins (β-lactoglobulin) were used as emulsifiers. In another study [115], SPG membrane was cleaned by sonication in acetone for 15 min and after that left in acetone for some days, heat-treated at 500°C for half an hour, and then stored. A dry membrane should be re-sonicated in water for 15 min prior to use to remove air trapped in pores. Alliod et al [116] reported rapid methods for cleaning hydrophilic and hydrophobic SPG membranes used for O/W and W/O nanoemulsions, respectively. For hydrophilic membrane with a pore size of 0.5 μm and an effective surface area of 30.7 cm^2, 500 ml of 1% Derquim+ (a commercial cleaning agent composed of biodegradable ionic and non-ionic surfactants) was passed through the contaminated membrane three times at 200 $ml \cdot min^{-1}$ and 70°C, followed by passing 500 mL of pure water three times at 200 $ml \cdot min^{-1}$ and room temperature. For hydrophobic membrane, a pure continuous phase (Marcol 82 mineral oil containing Span 80) was passed through the membrane until a clear solution was obtained and pressure stabilized. Jing et al [25] developed a successful cleaning procedure for ZrO_2 and α-Al_2O_3 ceramic membranes used for the preparation of SDS-stabilized O/W emulsions. The membranes were cleaned by passing 100 ml of ethanol and then 200 ml of 1 wt% NaOH through the membrane at 2 bar pressure at room temperature. Finally, the membrane was rinsed with hot water (70°C) at 1 bar pressure. After cleaning, the permeate flux was almost restored to its original value.

The membranes with smaller mechanical stability like polymeric membranes have a limited operational life, especially when working at high transmembrane pressures. The polymeric membranes are prone to fatigue or

disintegration after repeated emulsification cycles. A pressure-induced disintegration of the pores depends on the nature of the polymeric membranes. For instance, MCE membranes showed a higher fatigue level compared to PES membranes, as indicated by environmental scanning electron microscopic images [117]. The membrane skeleton could be broken down resulting in a net increase in pore size. Apart from the inherent properties of the membranes, emulsion formulation and prevailing flow conditions could also foster membrane disintegration. Moreover, as polymeric membranes are usually flexible, they can undergo compaction during emulsification process with a typical thickness reduction of 30% reported for MCE membranes [118], which can influence droplet breakup and production rates in PME. For this reason, polymeric membranes reported in PME studies were often used as disposable filters. Trentin et al [58] compared different cleaning protocols for a commercial (Whatman®) nylon membrane with a pore size of 0.8 μm that was used for the preparation of food-grade O/W emulsions containing whey proteins. Aqueous solutions of three agents, namely Derquim+ (pH 9.2), NaOH (pH 12.2), and Tween 20 (pH 5.4) were used either alone or in mixtures at different pressures and temperatures. The highest flux recovery (~60%) was achieved using 2 wt% Derquim+ alone through backwashing at 5 bar pressure at room temperature, followed by a mixture of 2 wt% Derquim+ and 2 wt% NaOH at 50°C. Regardless of the cleaning agent used, the increase in concentration of cleaning agent had a smaller effect on water flux recovery than backwash pressure. The water flux could not be fully recovered after cleaning due to membrane compaction under high applied pressure (9 bar), which probably have also made them less accessible to cleaning agent.

Similar to glass and ceramic membranes, the metallic membranes are reusable, have longer operational life, and must be cleaned after PME process due to high fabrication costs. However, as metallic membranes usually have straight-through pores, the extent of fouling is low compared to ceramic or polymeric membranes with highly branched pore network. In case of nickel microsieves with slotted pores [62, 64] cleaning can be carried out by flushing with tap water followed by cleaning with ethanol in an ultrasound bath for about 5 min. Nickel and stainless-steel membranes can withstand strong cleaning reagents, and therefore, commonly used acid-base cleaning can be carried out at wide range of pressure and temperature conditions. Santos et al [65] reported a cleaning protocol for the nickel micro-sieves having cylindrical pores (10 and 20 μm), which were used for the preparation of O/W emulsions. The membranes were cleaned in an ultrasonic bath, first in 4 M NaOH solution and then in 2 wt % citric acid solution, for 5 min each. The same acid-base cleaning protocol was adopted by Kaade et al [101] for cleaning nickel micro-sieves (having square-like and rectangular pores) used for the preparation of O/W

emulsions with Tween 20 as surfactant. The pore morphology was observed by scanning electron microscope after 5 consecutive emulsification cycles at 1.5 bar, followed by membrane cleaning and water flux measurement. The pores were damaged even after one full cycle, due to combined action of NaOH/citric acid cleaning and high shear during emulsification, as no changes in pore morphology were observed when the cleaning protocol was repeated 4 times on brand-new sieves without emulsification. However, the pore damage during the emulsification-cleaning cycle was reduced when acid treatment was removed from the cleaning protocol.

7. Conclusions and future prospects

Premix membrane emulsification (PME) is a robust process for the preparation of emulsions based on flow-induced breakup of large droplets within membrane pores. Over the last decade, it has been successfully used for the preparation of complex encapsulation matrices, such as double emulsions [18, 95], double emulsion-templated microspheres with porous structures [24, 45, 119], nanoemulsions [11], micro-/nanoparticles [120], colloidosomes [121], microgels [122], emulgels [123], high-energized composite materials [124], and droplets with multi-layered interface [115], after combining with suitable chemical and physicochemical processes (e.g., solvent evaporation, spray drying, free radical polymerization, ionic crosslinking, melt cooling, electrostatic deposition of oppositely charged polymers, complex coacervation, etc. [125]. The simplicity of design, the adaptability to a range of process and formulation conditions and the ability to generate submicron particles (easier than in DME) endorse a wider scope of PME. The availability of different types of membranes or porous media adds further to inherent flexibility of the process (Table 3). For instance, a more intense droplet disruption can be achieved by using membranes with interconnected pores and higher thickness, or otherwise, thin microsieves having straight-through rectangular pores could be used to get higher throughputs [62]. Disposable syringe filters can be used to handle small volumes, and to ensure sterile conditions during emulsification [126]. Furthermore, to produce W/O emulsions one can use polymeric membranes that are inherently hydrophobic without following any prior surface modification procedure [60].

Table 3. A comparison of different PME systems in terms of 5-star rating.

PME systems	Cost effective	Lifespan	Droplet size & uniformity	Throughput	Fouling resistance/mitigation
Glass membranes	★★★☆☆	★★★☆☆	★★★★★	★★★★☆	★★★☆☆
Ceramic membranes	★★★☆☆	★★★★☆	★★★★★	★★★★☆	★★★☆☆

Polymeric membranes (track-etched)	★★★★★	★★☆☆☆	★★★★★	★★★★★	★★★★☆
Metallic membranes	★★☆☆☆	★★★★★	★★★☆☆	★★★★★	★★★★☆
Unconsolidated porous media	★★★★★	★★★★★	★★★★☆	★★★☆☆	★★★★★

The required droplet size in a PME process can be easily tuned by selecting appropriate pore size and adjusting all relevant process parameters. Submicron droplets can be generated using low energy inputs, which allows preserving shear sensitive ingredients. A complete understanding of the droplet breakup in PME, especially in complex membrane structures, is still lacking. Different droplet breakup mechanisms may operate depending upon membrane morphology, initial droplet size, emulsion formulation, and prevailing flow conditions. The final droplet size is an interplay of various disruption forces and mechanisms that are quite difficult to quantify due to many interactions between different parameters. Various attempts have been made to establish scaling laws to predict final droplet size for some specific systems, but a generalized correlation is still missing. The most common approach is to use energy density and dimensionless numbers to describe the energy input, flow behavior and droplet disruption. Such expressions are available for specific PME systems and can fairly predict droplet size under prevailing flow conditions. Scaling relations based on advanced numerical methods are also available with high predictive power, but only for idealized pore geometries.

Undoubtedly, PME has a track-record of multifaceted applications but all in lab-scale experimental studies. The future research should be focused on different approaches for scaling-up PME manufacturing processes, for instance, using membrane with larger effective surface area or using several membrane modules in parallel. Additionally, for industrial applications, a continuous flow processing is more suitable that batch production. This would certainly assist in replacing conventional emulsification devices with PME systems in allied industries. Production capacity can also be increased by maximising transmembrane pressure at constant membrane surface area. Many types of conventional high-pressure homogenisers can be adopted for PME by replacing a standard homogenising valve with a high-pressure membrane extruder. For example, membrane extruder attachments can be used in line with Avestin EmulsiFlex homogenisers to achieve pressures up to 448 bar and a flow-through capacity up to 1,000 l/h. However, the limiting factor here is the ability of membrane to withstand high pressures. The maximum pressure tested in PME using a commercial Whatman Nuclepore™ track-etched polycarbonate

membrane with a pore size of 200 nm was 40 bar [33] and the maximum pressure applied in SPG membrane was 60 bar [82].

Industrial-scale production capacities can also be achieved by implementing specific hydrodynamic conditions that can enhance shear forces and droplet disruption. Recently, Micropore Technologies developed a high-throughput continuous flow DME device using a very narrow annular flow channel through which the continuous phase flows [67]. However, annular crossflow devices are not yet used to PME. In addition, low-pulse back-and-forward continuous phase flow oscillations have been used successfully in DME to decouple the shear required to detach droplets from the membrane surface from the shear provided by the crossflow to remove the product [127]. Perhaps, back-and-forward oscillations of feed emulsion can be implemented in PME to achieve higher throughputs because membranes with larger pore sizes can be used due to more efficient droplet disruption.

Appendix

Table A.1. Production of different materials through PME using SPG membranes.

Membrane characteristics D_m = membrane diameter L_m = membrane length X_m = membrane thickness d_p = pore diameter ε = membrane porosity ξ = pore tortuosity	**Product type and composition** O = oil W = water	**Droplet characteristics under optimum conditions** d_{32}, d_{43}, d_{50}, or d = Sauter, De Brouckere, median or generic droplet/particle diameter δ = span of distribution CV = coefficient of variation PDI = polydispersity index η_c = continuous phase viscosity	**Process parameters** Δp = applied pressure J = transmembrane flux N = number of extrusion cycles T = temperature	**Ref.**
Preparation of microemulsions				
Tubular, hydrophilic D_m = 8.5 mm; X_m = 0.8 mm; d_p = 8 μm; ε = 55%; ξ = 1.28	O/W microemulsion O = corn oil (40% of emulsion) W = water + emulsifier: Tween 20 (0.1-2 wt.%), SDS (0.06-2 wt.%), or β-Lg (0.5 or 2 wt.%)	d_{50} = 5.1 μm, CV = 27%, δ = 0.73 @ 0.5 wt.% SDS d_{50} = 6.6 μm, CV = 12%, δ = 0.33 @ 0.5 wt.% Tween 20 d_{50} = 10.9 μm, CV = 31%, δ = 0.73 @ 2 wt.% β-Lg	Δp = 100 kPa J = 3–60 $m^3m^{-2}h^{-1}$ N = 5 T = 295 K	[111]
Tubular, hydrophilic D_m = 8.5 mm; X_m = 0.8 mm; d_p = 8 μm	O/W microemulsion O = corn oil (10 or 20% of emulsion) W = water + acetic acid (100 mM) + NaN_3 (0.02 wt.%) + lecithin (1.6 or 1.8 wt.%)	d_{32} ≈ 5 μm	Δp = 100–150 kPa J = 30–1 $m^3m^{-2}h^{-1}$	[128]
Tubular, hydrophilic D_m = 10 mm; L_m = 125 mm; X_m = 0.8 mm; d_p = 10 μm	O/W microemulsion O = sunflower oil (20% of emulsion) W = water + WPI (1.0 wt.%) or WPI (0.5 wt.%)–CMC (0.25 wt.%)	d_{43} ≈ 10 μm δ = 1.7 (WPI) and 2.5 (WPI-CMC)	Δp = 150-200 kPa (WPI) Δp = 700-800 kPa (WPI-CMC)	[115]
Tubular, hydrophobic D_m = 10 mm; L_m = 20 mm; d_p = 10.2 μm; ε = 34%; ξ = 1.28	W/O microemulsion W = water + agarose (10 wt.%) + NaCl (0.9 wt.%) O = liquid paraffin/petroleum ether (7:5 v/v) + hexaglycerin penta ester (4 wt.%)	d = 10 μm	Δp = 98 N = 3	[122]
Preparation of nanoemulsions				
Tubular, hydrophilic D_m = 8.5 mm; L_m = 20 or 125 mm; X_m = 0.8 mm; d_p = 0.2, 0.3, 0.4, 0.5, 0.6 and 0.8 μm	O/W nanoemulsion O = ethylhexyl palmitate (10%) + span 80 (3.1%) W = water (85%) + Tween 20 (1.9%) Dispersed phase content = 5-40% Total surfactant concentration = 2.5-20%	d_{50} = 260 μm (for d_p = 0.2 μm)	J = 5 ml·min^{-1} (Δp = 6000 kPa), for d_p = 0.2 μm N = 1	[82]
Tubular, hydrophilic D_m = 8.5 mm; L_m = 125 mm; X_m = 0.8 mm; d_p = 0.5 μm	O/W nanoemulsion O = mineral oil: WMO, Marcol 82 or Marcol 52 (10%) + Span 80 (2.7%)	d_{50} = 293-673 nm, as function of η_c	J = 100 ml·min^{-1} (Δp = 1000-2000 kPa), as function of η_c N = 1	[116]

	W = water (85%) + Tween 20 (2.3%) +/- glycerol Dispersed phase content = 5-30% Glycerol content in water = 0-62.5%			
Tubular, hydrophobic D_m = 8.5 mm; L_m = 125 mm; X_m = 0.8 mm; d_p = 0.5 μm	W/O nanoemulsion W = water (10%) + Tween 20 (0.28%) +/- glycerol O = mineral oil: WMO, Marcol 82 or Marcol 52 (85%) + Span 80 (4.72%) Dispersed phase content = 1-15% Glycerol content in water = 0-100%	d_{50} = 550-650 nm, as function of η_c	J = 40-50 ml·min^{-1} (Δp = 2500-4500 kPa), as function of η_c N = 1	[116]
Preparation of double emulsions				
Tubular, hydrophilic D_m = 8.5 mm; X_m = 0.8 mm, d_p = 10.7 μm; ε = 55.2%; ξ = 1.3	$W_1/O/W_2$ emulsion W_1 = water + D-glucose (5 wt.%) O = soybean oil + PGPR (5 wt.%) W_2 = water + Tween 80 (0.5 wt.%) + D-glucose (5 wt.%) + sodium alginate (1 wt.%) W_1 in W_1/O = 10-30 vol.% W_1/O in $W_1/O/W_2$ = 1-60 vol.%	d_{50} (W_1/O) = 0·37-0·54 μm d_{50} (O/W_2) = 4·4-13·2 μm δ = 0.28-0.6	Δp = 20–300 kPa J = 1.8–37 m^{3}m^{-2}h^{-1} N = 5	[18]
Tubular, hydrophilic D_m = 8.5 mm; X_m = 0.8 mm; d_p = 20.3, 14.7, 10.7, 7.6, and 5.4 μm; ε = 50 - 58%; ξ = 1.2-1.3	$W_1/O/W_2$ emulsion W_1 = water + D-glucose (5 wt.%) + $CaNa_2$-EDTA (5 wt.%) O = soybean oil + PGPR (5 wt.%) W_2 = water + Tween 80 (0.5 wt.%) + D-glucose (5 wt.%) + sod. alginate (1 wt.%) W_1 in W_1/O = 0-0.5 vol.% W_1/O in $W_1/O/W_2$ = 0.01-0.5 vol.%	d_{50} (W_1/O) = 0·54-0·75 μm d_{50} (O/W_2) = 6.75-13.8 μm δ = 0.28-0.34	Δp = 70–150 kPa J = up to 200 m^{3}m^{-2}h^{-1} N = 5	[95]
Tubular, hydrophilic D_m = 8.5 mm; L_m = 12 mm; X_m = 0.8 mm; d_p = 8 μm	$W_1/O/W_2$ emulsion W_1 = water +/- WPI O = corn oil + PGPR (8 wt.%) W_2 = water + Tween 20 (0.5 wt.%) + phosphate buffer (5 mM) + NaCl (100 mM) + NaN_3 (0.02 wt. %, pH 7) W_1/O in $W_1/O/W_2$ = 0.2 vol.%	d_{32} = 1.56 μm (No-WPI) d_{32} = 2.01 μm (WPI-no-Gel) d_{32} = 1.95 μm (WPI-Gel)	Δp = 100 J = 70 (No-WPI, n=5) J = 66 (WPI-no-Gel, n=5) J = 64 (WPI-Gel, n = 5) N = 5 T = 21 °C	[129]
Preparation of solid lipid micro-/nanoparticles (SLMP or SLNP)				
Tubular, hydrophilic D_m = 10 mm; L_m = 20 mm; X_m = 0.8 mm; d_p = 5.4, 7.6, 9.9, and 14.8 μm; ε = 53–58%	Vitamin B_{12} loaded SLMP produced from $W_1/O/W_2$ emulsion W_1 = water + vitamin B_{12} (0.2-1.1 wt.%) O = glycerol trimyristate + PGPR (5 wt.%) W_2 = water + Tween 40 (1 wt.%) W_1/O in $W_1/O/W_2$ = 0.33 vol.%	d (S/O) = 68-132 nm d (O/W) = 10.5-15.5 μm δ = 0.48-0.67	Δp = 25–200 kPa J = ~10-140 m^{3}m^{-2}h^{-1} T = 60 °C	[130]

	W_1/O was transformed into S/O dispersion through water removal.			
Tubular, hydrophilic D_m = 10-11 mm; L_m = 20 mm; X_m = 0.7–0.9 mm; d_p = 0.1, 0.2, and 0.3 μm	SLNP produced from O/W emulsion O = trimyristin (10% of emulsion) W = water + surfactant (7.5%): SDS, poloxamer 188 or polysorbate 20	d_{50} = 100-200 nm	Δp = 900 kPa J = 10 ml in 8-30 min N = 1 T = ~65 °C	[125]
Preparation of biodegradable polymeric micro-/nanoparticles				
Tubular, hydrophilic d_p = 5.2 μm	HBsAg loaded PELA microparticles via $W_1/O/W_2$ emulsification and solvent evaporation W1 = water (0.4 ml) + HBsAg O = ethyl acetate (4 ml) + PELA: PLA, PLA-mPEG, or PLA-PEG-PLA (200 mg) W2 = water + PVA (1 wt./vol.%) + NaCl (1 wt./vol.%)	d = 1.0 μm CV = 18.9%	Δp = 300 kPa N = 1	[131]
Tubular, hydrophilic d_p = 50.2 μm	Exenatide loaded PLGA microparticles via $W_1/O/W_2$ emulsification and solvent evaporation W_1 = water (1 ml) + exenatide (30 mg) O = dichloromethane (8 ml) + PLGA (9.9 wt./vol.%) W_2 = water (80 ml) + PVA (2%) + NaCl (0.5 wt.%)	$d \approx$ 20 μm δ = 0.7	Δp = 5 kPa N = 3	[120]
Tubular, hydrophilic D_m = 8 mm; L_m = 170 mm; d_p = 5.2 and 7.2 μm	Hollow polylactone microparticles via $W_1/O/W_2$ emulsification and solvent evaporation W_1 = water (4 ml) O = dichloromethane (4 ml) + polylactone: PLLA, PLGA5050, PLGA7030, PEG-b-PLGA7030, PLC5050, PEG-b-PLLA (200 mg) W_2 = water + PVA (1 wt.%)	$d \approx$ 4 μm	Δp = 80 kPa N = 4	[132]
Tubular, hydrophilic d_p = 25.9 μm	Insulin loaded colloidosomes via $W_1/O/W_2$ emulsification and solvent extraction W_1 = water (200 μL) + acetic acid (2 vol.%) + insulin (4 mg) O = ethyl acetate (2 ml) + PLGA (5 wt.%) + Arlacel 83 (5 wt.%) W_2 = water (3 ml) + chitosan-coated alginate particles (1 wt.%) W_1/O in $W_1/O/W_2$ = 0.66 vol.%	$d \approx$ 9.1 μm CV = 23.2%	Δp = 11 kPa N = 5	[121]
Tubular, hydrophobic	Chitosan nanoparticles via W/O emulsification and solidification	d = 200-300 nm PDI = 0.027	Δp = 500-950 kPa N = 5	[133]

d_p = 1.4, 2.8, 5.2, 7.0, and 9.0 μm	W = water + chitosan (0.3-1 wt.%) O = liquid paraffin + petroleum ether + PO-500 (2-8 wt.%) W:O = 1:20-1:60			
Disc, hydrophilic d_p = 0.48, 1.00, 1.95 μm	PLGA nanoparticles via O/W emulsification and solvent evaporation O = acetone (10 ml) + PLGA7520 (1-5 wt./vol.%) W = water (90 ml) + PVA (1 wt.%)	d = 200 nm CV < 20%	$\Delta p \approx$ 2-11 kPa N = 1	[134]
Tubular, hydrophilic d_p = 2.1 μm	α-asarone loaded mPEG-PLA nanoparticles via O/W emulsification and solvent evaporation O = organic solvent + mPEG-PLA (13.5-22.5 mg/ml) W = water (5-9 ml) + PVA (10-20 mg/ml)	d = 355-370 nm PDI < 0.16	Δp = 900 kPa N =3	[135]

Where, PLA = poly(lactic acid); PLLA = poly(L-lactic acid); PELA = poly(lactide-co-ethylene glycol); PEG = poly(ethylene glycol); mPEG = methoxy poly(ethylene glycol); PLGA = poly(lactic-co-glycolic acid); PVA = poly (vinyl alcohol); HBsAg = hepatitis B surface antigen

Table A.2. The estimated values of the fit parameters of Eq. 8 and Eq. 9 for different PME systems.

Fit parameters	**Eq. 8, for PME system using metallic sieve (Fig. 7a) with long rectangular pores [64].**	**Eq. 9, for PME system using packed bed of glass spheres [69].**	
		$K_{\blacksquare}/K_{\shortparallel} > 3$	$K_{\blacksquare}/K_{\shortparallel} < 3$
α	16.59 ± 0.55	0.73 ± 0.031	0.57 ± 0.050
β	0.67 ± 0.04	0.31 ± 0.024	050 ± 0.061
γ	0.40 ± 0.05	0.35 ± 0.020	0.35 ± 0.020
ζ	-	0	0.16 ± 0.037

Where, η_d and η_c are the dispersed and continuous phase viscosities, respectively.

Table A.3. Best fit coefficients for the correlation of fluid dispersion, $\dot{\varphi}$, and mean Sauter droplet diameter, Ω_{32}.

	Fluid dispersion, $\dot{\varphi}$ (Eq. 10)				
	C_o	C_a	C_b	C_c	C_d
Non-spherical	1000	0.214	-1.252	0.053	-0.333
Spherical	1000	0.256	-1.147	-0.018	-0.066
	Mean Sauter droplet diameter, Ω_{32} (Eq. 11)				
	C_1	C_e	C_f	C_g	C_h
Non-spherical	1	-0.147	1.035	-0.395	3×10^{-8}
Spherical	1	-0.186	0.769	0.412	-2.8×10^{-4}

References

[1] McClements DJ. Food emulsions: principles, practices, and techniques: CRC press; 2015.

[2] Chappat M. Some applications of emulsions. Colloids Surf A 1994;91:57-77.

[3] McClements DJ, Decker EA, Weiss J. Emulsion-based delivery systems for lipophilic bioactive components. J Food Sci 2007;72:R109-R24.

[4] Anton N, Benoit J-P, Saulnier P. Design and production of nanoparticles formulated from nano-emulsion templates—A review. J Controlled Release 2008;128:185-99.

[5] Håkansson A. Emulsion formation by homogenization: Current understanding and future perspectives. Annual review of food science and technology 2019;10:239-58.

[6] Vladisavljevic GT, Kobayashi I, Nakajima M. Emulsion Formation in membrane and microfluidic devices. In: Tadros TF, (editor) Emulsion Formation and Stability, Wiley-VCH; 2013. Chapter 2.

[7] Cui P, Wang S. Application of microfluidic chip technology in pharmaceutical analysis: A review. Journal of pharmaceutical analysis 2019;9:238-47.

[8] Kukizaki M. Shirasu porous glass (SPG) membrane emulsification in the absence of shear flow at the membrane surface: influence of surfactant type and concentration, viscosities of dispersed and continuous phases, and transmembrane pressure. J Membr Sci 2009;327:234-43.

[9] Dragosavac MM, Sovilj MN, Kosvintsev SR, Holdich RG, Vladisavljevi GT. Controlled production of oil-in-water emulsions containing unrefined pumpkin seed oil using stirred cell membrane emulsification. J Membr Sci 2008;322:178-88.

[10] Nazir A, Schroën K, Boom R. Premix emulsification: A review. J Membr Sci 2010;362:1-11.

[11] Vladisavljević GT. Preparation of microemulsions and nanoemulsions by membrane emulsification. Colloids Surf A 2019;579:123709.

[12] Alliod O, Almouazen E, Nemer G, Fessi H, Charcosset C. Comparison of three processes for parenteral nanoemulsion production: ultrasounds, microfluidizer, and premix membrane emulsification. J Pharm Sci 2019;108:2708-2717.

[13] El-Hawari L, Bunjes H. Parameters influencing Ostwald ripening of nanoemulsions produced by premix membrane emulsification. SPhERe Proceedings: 3rd International Symposium on Pharmaceutical Engineering Research 2020.

[14] Gehrmann S, Bunjes H. Preparation of nanoemulsions by premix membrane emulsification: which parameters have a significant influence on the resulting particle size? J Pharm Sci 2017;106:2068-76.

[15] Suzuki K, Shuto I, Hagura Y. Characteristics of the membrane emulsification method combined with preliminary emulsification for preparing corn oil-in-water emulsions. Food Sci Technol Int 1996;2:43-7.

[16] Suzuki K, Fujiki I, Hagura Y. Preparation of corn oil/water and water/corn oil emulsions using PTFE membranes. Food Sci Technol Int 1998;4:164-7.

[17] Suzuki K, Hayakawa K, Hagura Y. Preparation of high concentration O/W and W/O emulsions by the membrane phase inversion emulsification using PTFE membranes. Food Sci Technol Res 1999;5:234-8.

[18] Vladisavljevic GT, Shimizu M, Nakashima T. Preparation of monodisperse multiple emulsions at high production rates by multi-stage premix membrane emulsification. J Membr Sci 2004;244:97-106.

[19] Van der Zwan EA, Schroën CGPH, Boom RM. Premix membrane emulsification by using a packed layer of glass beads. AIChE J 2008;54:2190-7.

[20] Li N, Sakaki K. Performance of an emulsion enzyme membrane reactor combined with premix membrane emulsification for lipase-catalyzed resolution of enantiomers. J Membr Sci 2008;314:183-92.

[21] Nazir A. Premix emulsification systems, PhD thesis, Wageningen University, Wageningen, The Netherlands 2013.

[22] Mugabi J, Naohiro K, Hiroki Y, Miki M, Igura N, Shimoda M. Preparation of small droplet size monodispersed emulsions at high production rate by continuous intramembrane premix emulsification method. J Chem Eng Japan 2019;52:259-66.

[23] Park SH, Yamaguchi T, Nakao S. Transport mechanism of deformable droplets in microfiltration of emulsions. Chem Eng Sci 2001;56:3539-48.

[24] Na X, Guo J, Li T, Zhou W, Ma G. Double emulsion-templated single-core PLGA microcapsules with narrow size distribution and controllable structure by using premix membrane emulsification. ChemNanoMat 2020;6:1059-62.

[25] Jing WH, Wu J, Xing WH, Jin WQ, Xu NP. Emulsions prepared by two-stage ceramic membrane jet-flow emulsification. AIChE J 2005;51:1339-45.

[26] Silva PS, Dragosavac MM, Vladisavljević GT, Bandulasena HCH, Holdich RG, Stillwell M, et al. Azimuthally oscillating membrane emulsification for controlled droplet production. AIChE J 2015;61:3607-15.

[27] Zou Y, Li S, Ngai T, Zhang S, Ma G, Wu J. Green preparation of hydrogel particles-in-emulsions for simultaneous enhancement of humoral and cell-mediated immunity. Eng Life Sci 2020;20:514-24.

[28] Jin H, Chong H, Zhu Y, Zhang M, Li X, Bazybek N, et al. Preparation and evaluation of amphipathic lipopeptide-loaded PLGA microspheres as sustained-release system for AIDS prevention. Eng Life Sci 2020;20:476-84.

[29] Liu Z, Lu Y, Zhang M, Wan W, Luo G. Controllable preparation of uniform polystyrene nanospheres with premix membrane emulsification. J Appl Polym Sci 2013;129:1202-11.

[30] Luhede L, Besser B, Schumacher D, Wilhelm M, Fritsching U. Continuous multistep encapsulation process for the generation of multiple emulsions. Chem Eng Technol 2021;44:15-22.

[31] López M, Rubio M, Sadek SH, Vega EJ. A simple emulsification technique for the production of micro-sized flexible powder of polydimethylsiloxane (PDMS). Powder Technol 2020;366:610-6.

[32] Pires PC, Peixoto D, Teixeira I, Rodrigues M, Alves G, Santos AO. Nanoemulsions and thermosensitive nanoemulgels of phenytoin and fosphenytoin for intranasal administration: Formulation development and in vitro characterization. Eur J Pharm Sci 2020;141:105099.

[33] Gehrmann S, Bunjes H. Instrumented small scale extruder to investigate the influence of process parameters during premix membrane emulsification. Chem Eng J 2016;284:716-23.

[34] Kukizaki M. Large-scale production of alkali-resistant Shirasu porous glass (SPG) membranes: Influence of ZrO2 addition on crystallization and phase separation in Na2O–CaO–Al2O3–B2O3–SiO2 glasses; and alkali durability and pore morphology of the membranes. J Membr Sci 2010;360:426-35.

[35] Vladisavljević GT. Fabrication of nanoemulsions by membrane emulsification. In Jafari SM, McClements DJ, (editors), Nanoemulsions. Academic Press; 2018. Chapter 10.

[36] Mi Y, Zhou W, Li Q, Gong F, Zhang R, Ma G, et al. Preparation of water-in-oil emulsions using a hydrophobic polymer membrane with 3D bicontinuous skeleton structure. J Membr Sci 2015;490:113-9.

[37] Mine Y, Shimizu M, Nakashima T. Preparation and stabilization of simple and multiple emulsions using a microporous glass membrane. Colloids Surf B 1996;6:261-268.

[38] Scherze I, Marzilger K, Muschiolik G. Emulsification using micro porous glass (MPG): surface behaviour of milk proteins. Colloids Surf B 1999;12:213-221.

[39] Song S-H, Cho Y-H, Park J. Microencapsulation of Lactobacillus casei YIT 9018 using a microporous glass membrane emulsification system. J Food Sci 2003;68:195-200.

[40] Vladisavljevic GT, Kobayashi I, Nakajima M, Williams RA, Shimizu M, Nakashima T. Shirasu porous glass membrane emulsification: characterisation of membrane structure by high-resolution X-ray microtomography and microscopic observation of droplet formation in real time. J Membr Sci 2007;302:243-53.

[41] Fan Q, Qi F, Miao C, Yue H, Gong F, Wu J, et al. Direct and controllable preparation of uniform PLGA particles with various shapes and surface morphologies. Colloids Surf A 2016;500:177-85.

[42] Lai EP, Wang YX, Wei Y, Li G. Preparation of uniform-sized and dual stimuli-responsive microspheres of poly(N-isopropylacrylamide)/poly(acrylic acid) with semi-IPN structure by one-step method. Polymers 2016;8.

[43] Wei Y, Wang Y, Zhang H, Zhou W, Ma G. A novel strategy for the preparation of porous microspheres and its application in peptide drug loading. J Colloid Interface Sci 2016;478:46-53.

[44] Li X, Wei Y, Lv P, Wu Y, Ogino K, Ma G. Preparation of ropivacaine loaded PLGA microspheres as controlled-release system with narrow size distribution and high loading efficiency. Colloids Surf A 2019;562:237-46.

[45] Na X, Zhou W, Li T, Hong D, Li J, Ma G. Preparation of double-emulsion-templated microspheres with controllable porous structures by premix membrane emulsification. Particuology 2019;44:22-7.

[46] Zhou QZ, Ma GH, Su ZG. Effect of membrane parameters on the size and uniformity in preparing agarose beads by premix membrane emulsification. J Membr Sci 2009;326:694-700.

[47] Nishihora RK, Luhede L, Fritsching U, Novy Quadri MG, Hotza D, Rezwan K, et al. Premix membrane emulsification using flat microfiltration inorganic membranes with tailored structure and composition. J Membr Sci 2020;608:118124.

[48] Nishihora RK, Rudolph E, Quadri MGN, Hotza D, Rezwan K, Wilhelm M. Asymmetric mullite membranes manufactured by phase-inversion tape casting from polymethylsiloxane and aluminum diacetate. J Membr Sci 2019;581:421-9.

[49] Joseph S, Bunjes H. Preparation of nanoemulsions and solid lipid nanoparticles by premix membrane emulsification. J Pharm Sci 2012;101: 2479-2489.

[50] Cheetangdee N, Fukada K. Protein stabilized oil-in-water emulsions modified by uniformity of size by premix membrane extrusion and their colloidal stability. Colloids Surf A 2012;403:54-61.

[51] Muhamad II, Quin CH, Selvakumaran S. Preparation and evaluation of water-in-soybean oil–in-water emulsions by repeated premix membrane emulsification method using cellulose acetate membrane. J Food Sci Technol 2015;53: 1845-1855.

[52] Gehrmann S, Bunjes H. Influence of membrane material on the production of colloidal emulsions by premix membrane emulsification. Eur J Pharm Biopharm 2018;126:140-8.

[53] Ramakrishnan S, Ferrando M, Aceña-Muñoz L, De Lamo-Castellví S, Güell C. Fish Oil Microcapsules from O/W Emulsions Produced by Premix Membrane Emulsification. Food Bioprocess Technol. 2013;6:3088-101.

[54] Trentin A, Ferrando M, López F, Güell C. Premix membrane O/W emulsification: effect of fouling when using BSA as emulsifier. Desalination 2009;245:388-395.

[55] Tan X, Rodrigue D. A review on porous polymeric membrane preparation. Part I: production techniques with polysulfone and poly (vinylidene fluoride). Polymers 2019;11:1160.

[56] Tan XM, Rodrigue D. A review on porous polymeric membrane preparation. Part II: Production techniques with polyethylene, polydimethylsiloxane, polypropylene, polyimide, and polytetrafluoroethylene. Polymers 2019;11:1160.

[57] Cheng J, Huang Q, Huang Y, Yu S, Xiao C, Hu Q. Pore structure design of NFES PTFE membrane for membrane emulsification. J Membr Sci 2020;611:118365.

[58] Trentin A, De Lamo S, Güell C, López F, Ferrando M. Protein-stabilized emulsions containing beta-carotene produced by premix membrane emulsification. J Food Eng 2011;106:267-74.

[59] Mi Y, Zhou W, Li Q, Zhang D, Zhang R, Ma G, Su Z. Detailed exploration of structure formation of an epoxy-based monolith with three-dimensional bicontinuous structure. RSC Advances 2015;5:55419-27.

[60] Mi Y, Li J, Zhou W, Zhang R, Ma G, Su Z. Improved stability of emulsions in preparation of uniform small-sized konjac glucomanna (KGM) microspheres with epoxy-based polymer membrane by premix membrane emulsification. Polymers 2016;8:53.

[61] Morelli S, Holdich RG, Dragosavac MM. Chitosan and Poly (Vinyl Alcohol) microparticles produced by membrane emulsification for encapsulation and pH controlled release. Chem Eng J 2016;288:451-60.

[62] Nazir A, Schroën K, Boom R. The effect of pore geometry on premix membrane emulsification using nickel sieves having uniform pores. Chem Eng Sci 2013;93:173-80.

[63] Kohnke M, Finke JH, Kwade A, Rösler J. Investigation of nanoporous superalloy membranes for the production of nanoemulsions. Metals 2018;8:361.

[64] Nazir A, Schroën K, Boom R. High-throughput premix membrane emulsification using nickel sieves having straight-through pores. J Membr Sci 2011;383:116-23.

[65] Santos J, Vladisavljević GT, Holdich RG, Dragosavac MM, Muñoz J. Controlled production of eco-friendly emulsions using direct and premix membrane emulsification. Chem Eng Research Design 2015;98:59-69.

[66] Geerken MJ, Groenendijk MNW, Lammertink RGH, Wessling M. Micro-fabricated metal nozzle plates used for water-in-oil and oil-in-water emulsification. J Membr Sci 2008;310:374-83.

[67] Holdich R, Dragosavac M, Williams B, Trotter S. High throughput membrane emulsification using a single-pass annular flow crossflow membrane. AIChE J 2020;66:e16958.

[68] Nazir A, Boom RM, Schroën K. Droplet break-up mechanism in premix emulsification using packed beds. Chem Eng Sci 2013;92:190-197.

[69] Nazir A, Boom RM, Schroën K. Influence of the emulsion formulation in premix emulsification using packed beds. Chem Eng Sci 2014;116:547-557.

[70] Ladjal Ettoumi Y, Berton-Carabin C, Chibane M, Schroën K. Legume Protein Isolates for Stable Acidic Emulsions Prepared by Premix Membrane Emulsification. Food Biophys 2017;12:119-128.

[71] Sahin S, Sawalha H, Schroën K. High throughput production of double emulsions using packed bed premix emulsification. Food Research Int 2014;66:78-85.

[72] Eisinaite V, Juraite D, Schroën K, Leskauskaite D. Preparation of stable food-grade double emulsions with a hybrid premix membrane emulsification system. Food Chem 2016;206:59-66.

[73] Sawalha H, Sahin S, Schroën K. Preparation of polylactide microcapsules at a high throughput with a packed-bed premix emulsification system. J Appl Polym Sci 2016;133:43536.

[74] Nazir A, Maan AA, Sahin S, Boom RM, Schroën K. Foam preparation at high-throughput using a novel packed bed system. Food Bioprod Process 2015;94:561-4.

[75] Gehrmann S, Bunjes H. Preparation of lipid nanoemulsions by premix membrane emulsification with disposable materials. Int J Pharm 2016;511:741-4.

[76] Kooiman K, Böhmer MR, Emmer M, Vos HJ, Chlon C, Shi WT, et al. Oil-filled polymer microcapsules for ultrasound-mediated delivery of lipophilic drugs. J Controlled Release 2009;133:109-18.

[77] Sawalha H, Fan Y, Schroën K, Boom R. Preparation of hollow polylactide microcapsules through premix membrane emulsification - effects of nonsolvent properties. J Membr Sci 2008;325:665-71.

[78] Sawalha H, Purwanti N, Rinzema A, Schroën K, Boom R. Polylactide microspheres prepared by premix membrane emulsification - effects of solvent removal rate. J Membr Sci 2008;310:484-93.

[79] Shima M, Kobayashi Y, Fujii T, Tanaka M, Kimura Y, Adachi S, Matsuno R. Preparation of fine W/O/W emulsion through membrane filtration of coarse W/O/W emulsion and disappearance of the inclusion of outer phase solution. Food Hydrocoll 2004;18:61-70.

[80] Nazzal FF, Wiesner MR. Microfiltration of oil-in-water emulsions. Water Environ. Res. 1996;68:1187-1191.

[81] Liang X, Wang X, Lu S, Wang K, Luo G. Pressure drop analysis for the droplet break-up flow in a locally constrictive microchannel. Chem Eng Sci 2021;230:116190.

[82] Alliod O, Valour J-P, Urbaniak S, Fessi H, Dupin D, Charcosset C. Preparation of oil-in-water nanoemulsions at large-scale using premix membrane emulsification and Shirasu Porous Glass (SPG) membranes. Colloids Surf A 2018;557:76-84.

[83] Melich R, Zorgani A, Padilla F, Charcosset C. Preparation of perfluorocarbon emulsions by premix membrane emulsification for Acoustic Droplet Vaporization (ADV) in biomedical applications. Biomed Microdevices. 2020;22:62.

[84] Wei Y, Wu Y, Wen K, Bazybek N, Ma G. Recent research and development of local anesthetic-loaded microspheres. Journal of Materials Chemistry B 2020;8:6322-6332.

[85] Liang Q, Xiang H, Li X, Luo C, Ma X, Zhao W, Chen J, Tian Z, Li X, Song X. Development of Rifapentine-Loaded PLGA-Based Nanoparticles: In vitro Characterisation and in vivo Study in Mice, Int J Nanomed 2020;15: 7491–7507.

[86] Van der Zwan E, Schroën K, van Dijke K, Boom R. Visualization of droplet break-up in pre-mix membrane emulsification using microfluidic devices. Colloids Surf A 2006;277:223-229.

[87] Karbstein H, Schubert H. Developments in the continuous mechanical production of oil-in-water macro-emulsions. Chem Eng Process 1995;34:205-211.

[88] Zhu L, Li Q, Gong F-L, Yan X-F, Li X-Q, Ma G-H, et al. An insight into structure regulation of uniform polystyrene micro/nano-particles by porogen in premix membrane emulsification process. J Membr Sci 2013;448:248-55.

[89] Wang J, Martínez-Hernández A, de Lamo-Castellví S, Romero M-P, Kaade W, Ferrando M, et al. Low-energy membrane-based processes to concentrate and encapsulate polyphenols from carob pulp. J Food Eng 2020;281:109996.

[90] Suraphan N, Fan L, Liu B, Wu D. Co-delivery of chlorantraniliprole and avermectin with a polylactide microcapsule formulation. RSC Advances 2020;10:25418-25.

[91] Mao S, Xu J, Cai C, Germershaus O, Schaper A, Kissel T. Effect of WOW process parameters on morphology and burst release of FITC-dextran loaded PLGA microspheres. Int J Pharm 2007;334:137-48.

[92] Vladisavljević GT. Recent advances in the production of controllable multiple emulsions using microfabricated devices. Particuology 2016.

[93] Shi Z, Lai X, Sun C, Zhang X, Zhang L, Pu Z, et al. Step emulsification in microfluidic droplet generation: mechanisms and structures. Chem Commun 2020;56:9056-9066.

[94] Hunter DG, Frisken BJ. Effect of Extrusion Pressure and Lipid Properties on the Size and Polydispersity of Lipid Vesicles. Biophys J 1998;74:2996-3002.

[95] Vladisavljevic GT, Shimizu M, Nakashima T. Production of multiple emulsions for drug delivery systems by repeated SPG membrane homogenization: influence of mean pore size, interfacial tension and continuous phase viscosity. J Membr Sci 2006;284:373-383.

[96] Nabavi SA, Gu S, Vladisavljević GT, Ekanem EE. Dynamics of double emulsion break-up in three phase glass capillary microfluidic devices. J Colloid Interface Sci 2015;450:279-287.

[97] Hornig N, Fritsching U. Liquid dispersion in premix emulsification within porous membrane structures. J Membr Sci 2016;514:574-85.

[98] Wollborn T, Luhede L, Fritsching U. Evaluating interfacial shear and strain stress during droplet deformation in micro-pores. Phys Fluids. 2019;31.

[99] Navarro R, Maristany A, Davis RH. Simulation of drop motion and breakup in narrow pores. Chem Eng Sci 2021;229:116057.

[100] Güell C, Ferrando M, Trentin A, Schroën K. Apparent interfacial tension effects in protein stabilized emulsions prepared with microstructured systems. Membr 2017;7:19.

[101] Kaade W, Ferrando M, Khanmohammed A, Torras C, De Lamo-Castellví S, Güell C. Low-energy high-throughput emulsification with nickel micro-sieves for essential oils encapsulation. J Food Eng 2019;263:326-36.

[102] Kaade W, Güell C, Ballon A, Mellado-Carretero J, De Lamo-Castellví S, Ferrando M. Dynamic membranes of tunable pore size for lemon oil encapsulation. LWT 2020;123:109090.

[103] Schroën K, Ferrando M, de Lamo-Castellví S, Sahin S, Güell C. Linking Findings in Microfluidics to Membrane Emulsification Process Design: The Importance of Wettability and Component Interactions with Interfaces. Membr 2016;6:26.

[104] Cerdeira AT, Campos JB, Miranda JM, Araújo JDJM. Review on microbubbles and microdroplets flowing through microfluidic geometrical elements. Micromachines, 2020;11:201.

[105] Salama A. Investigation of the onset of the breakup of a permeating oil droplet at a membrane surface in crossflow filtration: A new model and CFD verification. Int J Multiph Flow 2020;126:103255.

[106] Link DR, Anna SL, Weitz DA, Stone HA. Geometrically mediated breakup of drops in microfluidic devices. Phys Rev Lett 2004;92:054503.

[107] Protiere S, Bazant M, Weitz D, Stone HAJE. Droplet breakup in flow past an obstacle: A capillary instability due to permeability variations. Europhys Lett 2010;92:54002.

[108] Xu Q, Nakajima M. Generation of droplets in flow focusing microfluidic devices. Seminar held in Nakajima Lab, NFRI 2015.

[109] Liu J, Yap YF, Nguyen N-T. Behavior of microdroplets in diffuser/nozzle structures. Microfluid Nanofluid 2009;6:835-46.

[110] Wang X, Wang K, Riaud A, Wang X, Luo G. Experimental study of liquid/liquid second-dispersion process in constrictive microchannels. Chem Eng J 2014;254:443-451.

[111] Vladisavljevic GT, Surh J, McClements JD. Effect of emulsifier type on droplet disruption in repeated Shirasu porous glass membrane homogenization. Langmuir 2006;22:4526-33.

[112] Silalahi SHD, Leiknes T. Cleaning strategies in ceramic microfiltration membranes fouled by oil and particulate matter in produced water. Desalination 2009;236:160-9.

[113] Tummons E, Han Q, Tanudjaja HJ, Hejase CA, Chew JW, Tarabara VV. Membrane fouling by emulsified oil: A review. Sep Purif Technol 2020;248:116919.

[114] Trentin A, Güell C, Gelaw T, De Lamo S, Ferrando M. Cleaning protocols for organic microfiltration membranes used in premix membrane emulsification. Sep Purif Technol 2012;88:70-8.

[115] Berendsen R, Güell C, Henry O, Ferrando M. Premix membrane emulsification to produce oil-in-water emulsions stabilized with various interfacial structures of whey protein and carboxymethyl cellulose. Food Hydrocoll 2014;38:1-10.

[116] Alliod O, Messager L, Fessi H, Dupin D, Charcosset C. Influence of viscosity for oil-in-water and water-in-oil nanoemulsions production by SPG premix membrane emulsification. Chem Eng Res Design 2019:87-99.

[117] Trentin A, Güell C, López F, Ferrando M. Microfiltration membranes to produce BSA-stabilized O/W emulsions by premix membrane emulsification. J Membr Sci 2010;356:22-32.

[118] Aghajani M, Maruf SH, Wang M, Yoshimura J, Pichorim G, Greenberg A, et al. Relationship between permeation and deformation for porous membranes. J Membr Sci 2017;526:293-300.

[119] Zhang B, Yang T, Wang Q, Zhang G, Huo J, Huang J, et al. Fabrication of uniform alginate-agarose microcapsules loading FeSO4 using water-oil-water-oil multiple emulsions system combined with premix membrane emulsification technique. Colloids Surf A 2016;498:128-38.

[120] Qi F, Wu J, Fan Q, He F, Tian G, Yang T, et al. Preparation of uniform-sized exenatide-loaded PLGA microspheres as long-effective release system with high encapsulation efficiency and bio-stability. Colloids Surf B 2013;112:492-8.

[121] Nan F, Wu J, Qi F, Fan Q, Ma G, Ngai T. Preparation of uniform-sized colloidosomes based on chitosan-coated alginate particles and its application for oral insulin delivery. J Mater Chem B 2014;2:7403-9.

[122] Zhou QZ, Wang LY, Ma GH, Su ZG. Multi-stage premix membrane emulsification for preparation of agarose microbeads with uniform size. J Membr Sci 2008;322:98-104.

[123] Santos J, Calero N, García-Capitán J, Muñoz J. Preparation and characterization of emulgels loaded with sweet fennel oil. J Dispers Sci Technol 2020;41:1381-9.

[124] Wang J, An C, Ye B, Xu R, Liu Q, Wang J, Dong J. CL-20/CAB energetic composite microspheres prepared by premix membrane emulsification. AIP Adv 2020;10:125005.

[125] Vladisavljević GT. Structured microparticles with tailored properties produced by membrane. Adv Colloid Interf Sci 2015;225;53-87.

[126] Joseph S, Bunjes H. Evaluation of Shirasu Porous Glass (SPG) membrane emulsification for the preparation of colloidal lipid drug carrier dispersions. Eur J Pharm Biopharm 2014;87:178-86.

[127] Holdich RG, Dragosavac M, Vladisavljević, GT, Piacentini, E. Continuous membrane emulsification with pulsed (oscillatory) flow. Ind Eng Chem Res 2013;52:507-515.

[128] Surh J, Jeong YG, Vladisavljević GT. On the preparation of lecithin-stabilized oil-in-water emulsions by multi-stage premix membrane emulsification. J Food Eng 2008;89:164-70.

[129] Surh J, Vladisavljevic GT, Mun S, McClements DJ. Preparation and characterization of water/oil and water/oil/water emulsions containing biopolymer-gelled water droplets. J Agric Food Chem 2007;55:175-84.

[130] Kukizaki M. Preparation of solid lipid microcapsules via solid-in-oil-in-water dispersions by premix membrane emulsification. Chem Eng J 2009;151:387-96.

[131] Wei Q, Wei W, Tian R, Wang Ly, Su ZG, Ma GH. Preparation of uniform-sized PELA microspheres with high encapsulation efficiency of antigen by premix membrane emulsification. J Colloid Interface Sci. 2008;323:267-73.

[132] Liu B, Zhou X, Yang F, Shen H, Wang S, Zhang B, et al. Fabrication of uniform sized polylactone microcapsules by premix membrane emulsification for ultrasound imaging. Polym Chem 2014;5:1693-701.

[133] Lv P-P, Wei W, Gong F-L, Zhang Y-L, Zhao H-Y, Lei J-D, et al. Preparation of uniformly sized chitosan nanospheres by a premix membrane emulsification technique. Ind Eng Chem Res 2009;48:8819-28.

[134] Ito F, Kanakubo Y, Murakami Y. Rapid preparation of monodisperse biodegradable polymer nanospheres using a membrane emulsification technique under low gas pressure. J Polym Res 2011:1-9.

[135] Pan L, Zhou J, Ju F, Zhu H. Intranasal delivery of α-asarone to the brain with lactoferrin-modified mPEG-PLA nanoparticles prepared by premix membrane emulsification. Drug Deliv Transl Res 2018;8:83-96.